PERGAMON

Journal of Structural Geology 22 (2000) 1–23

JOURNAL OF STRUCTURAL GEOLOGY

www.elsevier.nl/locate/jstrugeo

Joints at high angles to normal fault strike: an explanation using 3-D numerical models of fault-perturbed stress fields ☆

Simon A. Kattenhorn*, [1], Atilla Aydin, David D. Pollard

Rock Fracture Project, Department of Geological and Environmental Sciences, Stanford University, Stanford, CA 94305, USA

Received 7 October 1998; accepted 12 July 1999

Abstract

Structural methods based on homogeneous stress states predict that joints growing in an extending crust form with strike orientations identical to normal faults. However, we document a field example where the strikes of genetically related normal faults and joints are almost mutually perpendicular. Field relationships allowed us to constrain the fracture sequence and tectonic environment for fault and joint growth. We hypothesize that fault slip can perturb the surrounding stress field in a manner that controls the orientations of induced secondary structures. Numerical models were used to examine the stress field around normal faults, taking into consideration the effects of 3-D fault shape, geometrical arrangement of overlapping faults, and a range of stress states. The calculated perturbed stress fields around model normal faults indicate that it is possible for joints to form at high angles to fault strike. Such joint growth may occur at the lateral tips of an isolated fault, but is most likely in a relay zone between overlapping faults. However, the angle between joints and faults is also influenced by the remote stress state, and is particularly sensitive to the ratio of fault-parallel to fault-perpendicular stress. As this ratio increases, joints can propagate away from faults at increasingly higher angles to fault strike. We conclude that the combined remote stress state and perturbed local stress field associated with overlapping fault geometries resulted in joint growth at high angles to normal fault strike at a field location in Arches National Park, Utah.

1. Introduction

Much of the understanding of joint orientations around normal faults follows from Anderson (1951), who indicated that opening mode cracks (specifically, dikes) should form parallel to the strikes of normal faults (perpendicular to the least compressive remote stress; Fig. 1a). Although this assumption provides a rationale for predicting fault orientations in extending crust, it does not incorporate the stress perturbation induced by growing faults and the consequences of this for joint growth close to faults (Fig. 1b). The fact that faults perturb the surrounding stress field during slip events (Pollard and Segall, 1987; Barton and Zoback, 1994) has important consequences for the orientations of secondary structures such as smaller faults, joints, veins, and solution surfaces.

Geological observations have established that secondary structures can be induced in regions of increased stress around both opening mode (mode I) cracks, such as dikes (Delaney and Pollard, 1981; Delaney et al., 1986; Pollard and Segall, 1987; Rogers and Bird, 1987; Baer and Reches, 1991; Kattenhorn and Watkeys, 1995) and sliding mode (modes II and III) cracks, such as faults (Lajtai, 1969; Segall and Pollard, 1980, 1983; Rispoli, 1981; Cruikshank et al., 1991; Rawnsley et al., 1992; Homberg et al., 1997; Ohlmacher and Aydin, 1997; Willemse et al., 1997; Martel and Boger, 1998; Vermilye and Scholz, 1998). Laboratory experiments that record acoustic emission events in a sample undergoing shear failure also reveal microcrack development ahead of a propagating fault tip (Reches and Lockner, 1994).

☆ Supplemental 3-D perspective color images of numerical model results may be viewed online at http://veo.elsevier.nl/sg/publish/831

* Corresponding author.

E-mail address: simkat@uidaho.edu (S.A. Kattenhorn).

[1] Present address: Department of Geology and Geological Engineering, University of Idaho, Moscow, ID 83844, USA.

0191-8141/00/$ - see front matter
PII: S0191-8141(99)00130-3

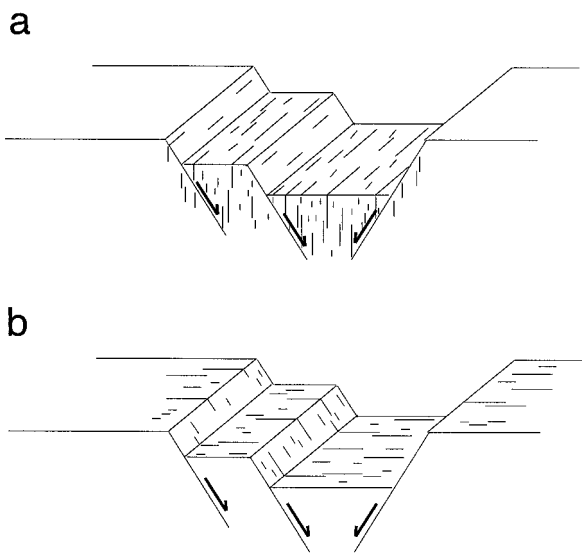

Fig. 1. (a) Anderson's (1951) prediction of relative joint and normal fault orientations. Joints are parallel to fault strike. (b) Contrasting fault and joint arrangement, with joints at high angles to normal fault strike.

If sufficient field evidence exists to suggest a genetic relationship between normal faults and spatially associated joints, joint orientations can perhaps be explained in the context of the fault-perturbed stress field. Joints act as paleostress indicators in rock and are assumed in this study to be mode I fractures that form perpendicular to the least compressive stress. Previous work on stress field heterogeneities around faults follows predominantly from field observations or modeling of either strike-slip or thrust faults (Barton and Zoback, 1994; Bürgmann et al., 1994; Roering et al., 1997). Our investigation focuses on the mechanics of stress perturbations by normal faulting and resultant joint development.

This study is motivated by observations of joints striking at high angles to normal faults in Arches National Park, Utah, in contrast to the predictions of Anderson (1951). First, the field example will be described to establish the connection between normal faults and joints. Second, we present three-dimensional mechanical analyses of the perturbed stress field in the vicinity of mechanically interacting, discontinuous normal faults. We then compare the numerical model results with field examples to demonstrate a similarity between model predictions and what is observed in nature, so as to provide a mechanical rationale for the field observations. Finally, we address implications of our model results for the analysis of deformation around normal faults in general and provide examples of applications.

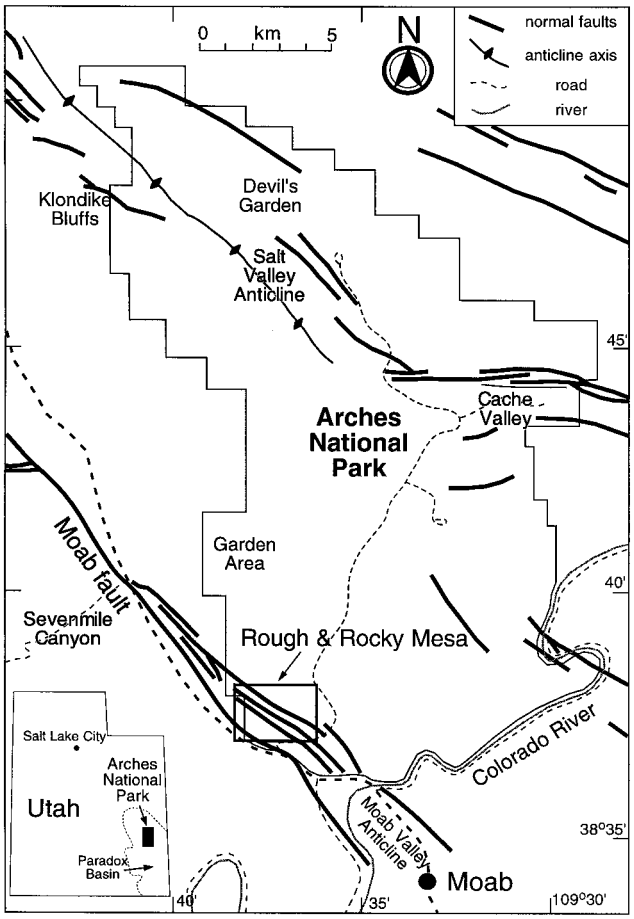

Fig. 2. Arches National Park region in southeastern Utah. The normal fault system at Rough and Rocky Mesa is in the southwest corner of the park. After Antonellini and Aydin (1995).

2. Faults and joints in sandstone

Exceptional surface exposure in many regions in the Colorado Plateau physiographic province of the USA, such as Arches National Park in southeastern Utah (Fig. 2), provides ideal locations for the study of joints and faults in sandstone. Prominent exposure of Jurassic sandstones in this region has inspired a number of investigations of fault and joint characteristics (locations shown in Fig. 2). Dyer (1983, 1988) investigated systematic joint domains on both flanks of the Salt Valley anticline. Cruikshank et al. (1991) and Zhao and Johnson (1992) examined the deformation history and the effects of shearing along pre-existing joints in the Garden Area. Cruikshank and Aydin (1995) determined the sequence of fracturing and characteristics of individually identifiable joint domains in the Klondike Bluffs region. Cruikshank and Aydin (1994) showed how joint clustering acts as a precursor to arch development in the park. Antonellini and Aydin (1994, 1995) and Antonellini et al. (1994a) examined the nature of faulting in sandstones in the

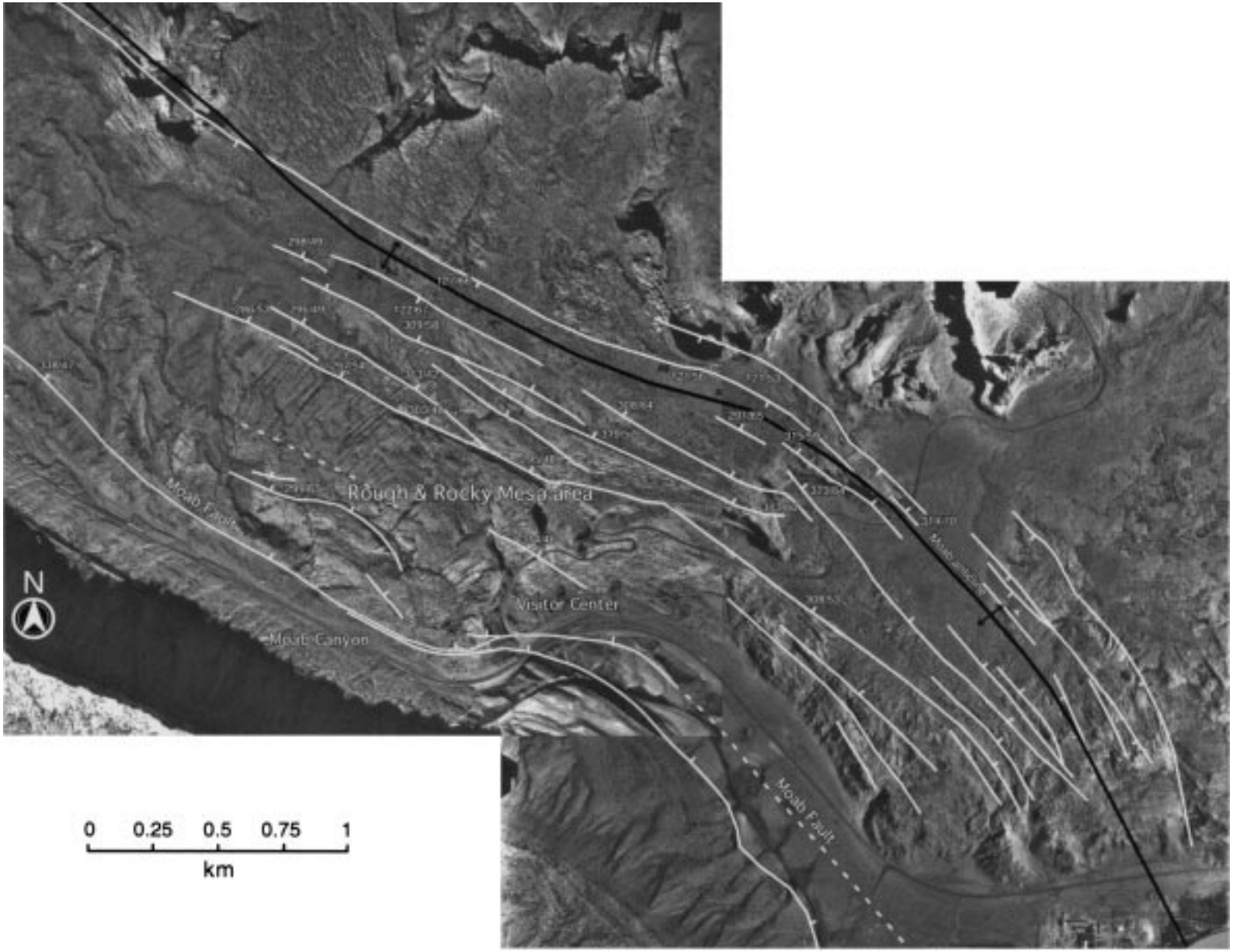

Fig. 3. Photo mosaic of the Rough and Rocky Mesa fault system (solid white lines with tick marks indicating downthrown block). The faults strike along the crest of the Moab Anticline (fold axial trace shown by black line) and are parallel to the adjacent Moab Fault. Joints in Jurassic sandstones are visible as eroded gullies. The aerial photos used are BLM AB4UPRM0005858A62 and AB4UPRM0001959A51.

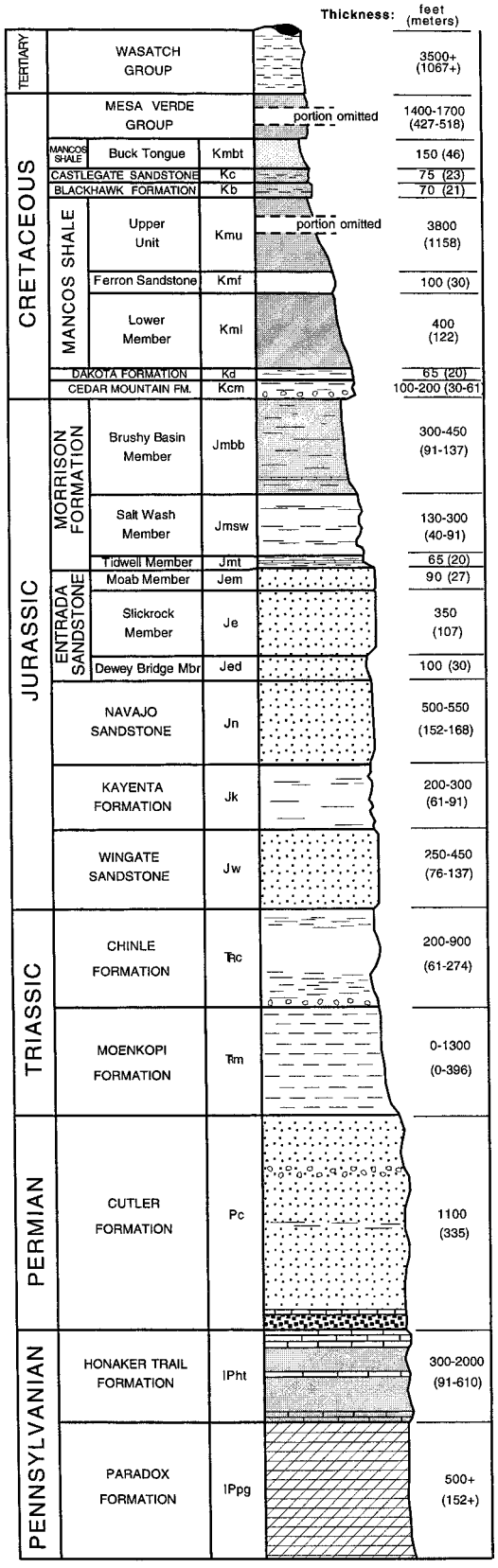

Fig. 4. Stratigraphic column showing units present in the Rough and Rocky Mesa region during normal faulting in the Tertiary. All units younger than the Brushy Basin Member of the Morrison Formation were subsequently removed by erosion in the Rough and Rocky Mesa region. After Doelling (1985).

Cache Valley region. These studies have considered joint development in response to either bending stresses within anticlines or slip patches along bedding planes during flexural slip folding. A detailed analysis of the relationship between normal faults and joints in Arches National Park is lacking.

An analysis of aerial photographs of Arches National Park and field reconnaissance has revealed a variety of orientations of joints that appear to be related to normal faulting. In this paper, we focus on an example of joints at high angles to normal fault strike in the Rough and Rocky Mesa region of the park (hereafter referred to as Rocky Mesa; Figs. 2 and 3).

The Arches National Park region is within the Paradox Basin, a fault-generated basin at the margin of the ancestral Uncompahgre uplift (Doelling et al., 1995). Rock units cropping out in the Rocky Mesa vicinity range from the Pennsylvanian Honaker Trail Formation to the Late Jurassic Morrison Formation (Fig. 4). The entire region is underlain by Pennsylvanian Paradox Formation salt, which crops out at breached salt-cored anticlines in Moab Valley to the southeast of Rocky Mesa, and Salt Valley to the north. The fault and joint outcrops are best developed in the Moab Member of the Jurassic Entrada Sandstone. Vertical cliffs along the southeastern edge of Rocky Mesa expose the underlying Slick Rock and Dewey Bridge Members, as well as the Navajo Sandstone, providing a means of estimating offsets along normal faults exposed in the cliff faces.

Joints in the Moab Member are zones of preferential erosion that formed deep, accessible gullies. This permits accurate identification of joint distribution and trends in aerial photos (Fig. 3), and the field-based characterization of 3-D joint orientations through most of the thickness of the unit.

2.1. Tectonic history

The tectonic evolution of the Paradox Basin and resultant structural trends follow from deposition of evaporites over pre-Pennsylvanian normal faulted basement (Baars and Stevenson, 1981; Baars and Doelling, 1987; Friedman et al., 1994). Periodic normal fault movement from the Pennsylvanian to the Tertiary, in conjunction with progressive sedimentary loading, induced salt migration towards fault zones (Shoemaker et al., 1958; Cater, 1970; Gard, 1976; Baars and Doelling, 1987; Doelling, 1988). Diapiric salt anticlines thus formed above and parallel to the basement faults, as is confirmed by borehole and seismic data (Doelling, 1988). Cretaceous and Tertiary units were incorporated into the existing fold trends during the Laramide orogeny: an approximately northeast-directed regional compressional tectonic event in the late Cretaceous to early Tertiary (Baars and

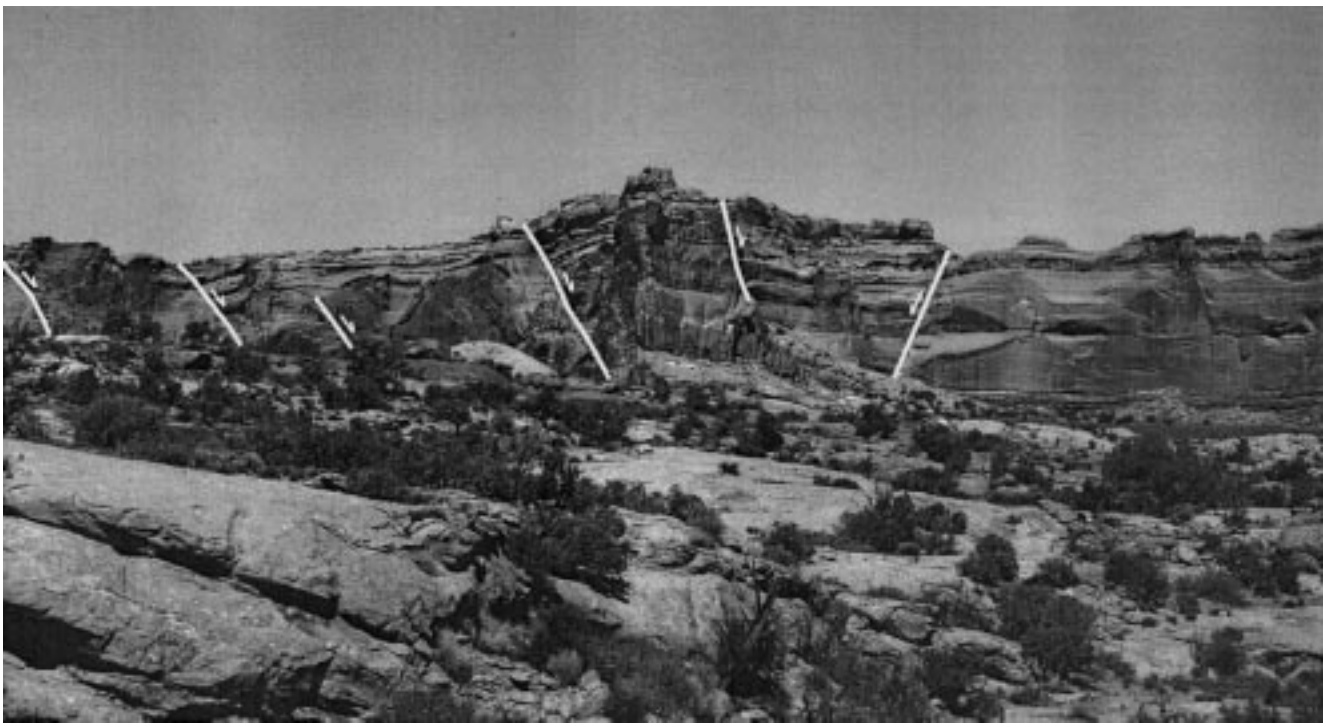

Fig. 5. Keystone-like collapse of the anticlinal crest of the Moab Anticline by normal faults. View to the northwest. Rough and Rocky Mesa is the area at the top of the cliff.

Stevenson, 1981; Doelling et al., 1995). This deformational event enhanced and possibly induced additional salt movement into pre-existing salt-cored anticlines, producing gentle folds in the southern Arches National Park area. Pliocene uplift of the Colorado Plateau exhumed salt structures, resulting in dissolution and collapse of salt-cored anticlines now manifested as northwest-trending valleys (Cater, 1970; Doelling, 1985; Huntoon, 1988), as well as causing the removal by erosion of Cretaceous and Tertiary sedimentary units in the Arches National Park area.

Rocky Mesa is located on the crest of the Moab Anticline (Fig. 3), about 4.5 km to the north of the Colorado River and Moab Valley. Rocky Mesa is topographically higher than Moab Valley by up to 250 m and has outcrops of stratigraphic units through to the Jurassic Morrison Formation (Fig. 4). A normal fault system trends parallel to the axis of the Moab Anticline, accommodating keystone-like collapse of the anticlinal crest (Fig. 5).

Rocky Mesa is bounded to the southwest by the Moab Fault: a 54-km-long, major normal fault that trends northwest along Moab Canyon (Figs. 2 and 3) and dips 50–75° NE (Foxford et al., 1996; Olig et al., 1996). The portion of the Moab Fault that passes adjacent to the Rocky Mesa region has the greatest total offset, which we estimate to be 815 m based on stratigraphic thicknesses along the length of the fault. Slip on the Moab Fault intensified hanging wall bending of the pre-existing Moab Anticline.

The Moab Fault cuts through exposed units as young as Cretaceous and has conventionally been assumed to have resulted from either post-Laramide relaxation in the Tertiary (McKnight, 1940; Baars and Doelling, 1987; Doelling, 1988; Olig et al., 1996) or Cenozoic salt-dissolution collapse (Huntoon, 1982; Hecker, 1993). Foxford et al. (1996) suggest the Moab Fault began growing in pre-Laramide time with recurrent episodes of slip since the Triassic. The Moab Fault is not currently active; indirect evidence of fault movement, such as geomorphic features, suggests that all fault motion was pre-Quaternary (Olig et al., 1996).

2.2. Normal fault characteristics

The Rocky Mesa normal faults along the crest of the Moab Anticline (Fig. 3) are northwest trending (291–319°) with fault dips ranging from 42 to 67°. Opposing fault dip directions on either side of the anticline crest indicate that faults dip towards the fold axial plane. Fault strikes undergo a small (~20°), clockwise rotation to the southeast of Rocky Mesa, corresponding to a left-stepping jog in the adjacent Moab Fault at the entrance to Arches National Park (Fig. 3). Fault lengths at Rocky Mesa range from around 0.25 to 4 km with spacings of 100–400 m; fault overlaps are variable (up to 30% of the fault length).

Fig. 6. Deformation band-style of normal faulting in the Moab Member of the Entrada Sandstone. Camera lens cap for scale (6 cm wide).

We concur with Doelling et al. (1994) that the Rocky Mesa normal faults are the result of bending stresses across the Moab Anticline. This bending and related deformation was likely enhanced by motion along the adjacent Moab Fault. Although exact measurements of fault offsets are not possible at the surface, stratigraphic juxtapositions indicate that most of the Rocky Mesa faults have approximate offsets on the order of only a few meters. The maximum recorded offset is 30 m where one of the faults crosses the entrance road to Arches National Park. The faults cut the stratigraphy at least as deep as the Wingate Sandstone and as shallow as the Salt Wash Member of the Morrison Formation (Fig. 4), indicating maximum down-dip fault heights of 670–875 m. The northeastern bounding fault of the system cuts as deep as the Chinle Formation at the Colorado River, and is an exception to the small-offset faults in that it has a documented offset of 152 m at that location (Fig. 3; Doelling et al., 1995).

In the Moab Member, the Rocky Mesa faults are manifested as zones of deformation bands (Aydin, 1978; Aydin and Johnson, 1978; Antonellini and Aydin, 1994, 1995; Antonellini et al., 1994a, b), generally < 2.5 m wide (Fig. 6). The evolutionary sequence of fault development is from a single deformation band to a zone of deformation bands to discrete slip surfaces [see Antonellini and Aydin (1995) for a detailed definition]. We use the term *fault* to imply a fully evolved structure exhibiting discrete slip surfaces. Deformation bands are ubiquitous in the Moab Member, with greatest density along the crest of the Moab Anticline (Fig. 7). The deformation bands define a conjugate set dipping either NE or SW that accommodates no more than a few millimeters to centimeters of offset. Slickensides on exposed slip surfaces indicate pure dip-slip motion on the Rocky Mesa faults. Most of these faults exhibit relatively constant strike trends, except for one fault immediately adjacent to the Moab Fault, which exhibits an arcuate map pattern and is in a zone of highly variable joint patterns associated with the Moab Fault (Figs. 3 and 7).

The timing relationship between Rocky Mesa normal faulting and the folding of the Moab Anticline during the Laramide compressional tectonic event (Cater, 1970) suggests that faulting of the folded Jurassic sandstone units at Rocky Mesa occurred no earlier than the late Cretaceous to early Tertiary. A major joint set emanating away from the Moab Fault in the Navajo Sandstone (Fig. 7) exhibits several slipped joints, manifest by gouge development along the joints. The joints in this vicinity are parallel to the jog in the Moab Fault at the park entrance, which shows slickenside evidence of having undergone right oblique-normal slip. Slip on these joints is thus interpreted to have been related to slip on the Moab Fault in the region of the fault jog. The slipped joints offset deformation bands associated with the Rocky Mesa normal fault system, indicating that these normal faults had formed prior to the cessation of slip on the Moab Fault in the late Tertiary.

In addition, the Rocky Mesa normal faults along the Moab Anticline are restricted to the location of maximum slip along the adjacent Moab Fault. As slip on the Moab Fault decreases towards the northwest, the Moab Anticline gradually disappears, as does the related faulting. This is evidence that the intensity of folding and related faulting was accentuated by slip along the Moab Fault no later than the late Tertiary, constraining the minimum age of Rocky Mesa faulting. The combination of these lines of evidence supports a Tertiary age for normal fault development at Rocky Mesa.

Estimates of the depth of burial during active faulting can be made from the previous timing inferences in conjunction with measured and referenced formation thicknesses in the vicinity. No units younger than mid-

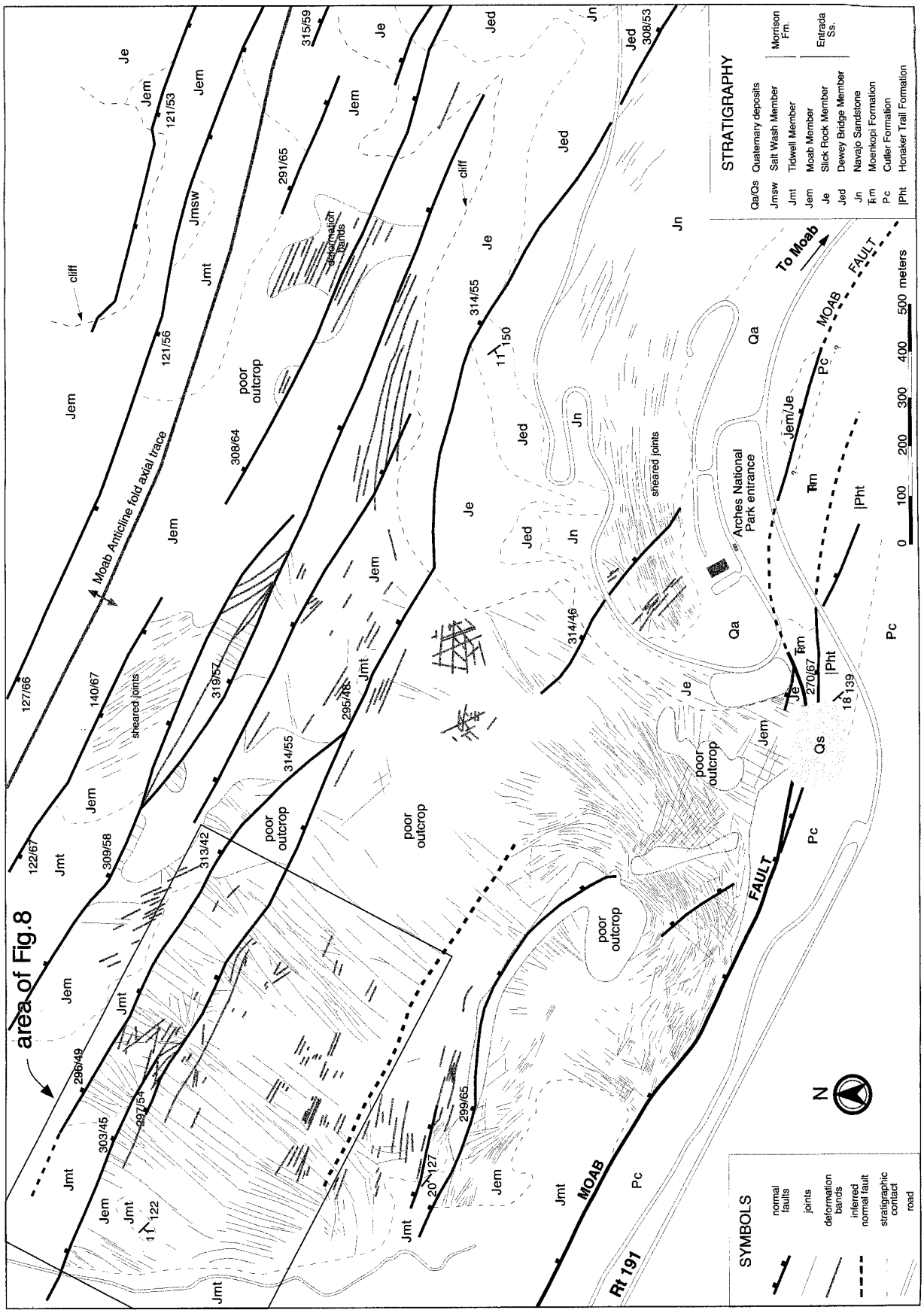

Fig. 7. Fault and joint map for Rough and Rocky Mesa. Normal faults parallel the axis of the Moab Anticline. Joints occur with a variety of orientations, including almost fault-perpendicular (box for Fig. 8). Some of the denser concentrations of deformation bands are shown, such as along the crest of the anticline. Tick marks along faults indicate the downthrown hanging wall. Numbers represent strikes and dips and utilize the right-hand rule.

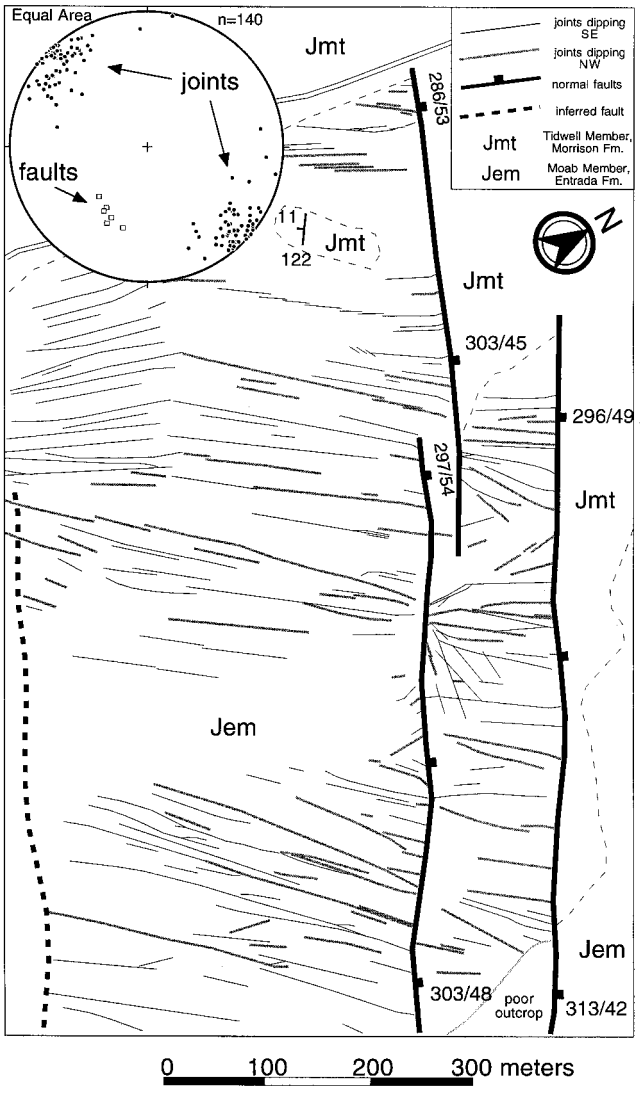

Fig. 8. Detailed joint map of the region where joints strike at high angles to the faults (box in Fig. 7). Joints dip steeply to either the northwest or the southeast. The dashed line is an inferred fault beneath the surface with an associated joint set at its northwestern tip. Inset: stereonet showing orientations of faults and joints. Most joints are nearly vertical, with decreases in dip towards the interface between the Moab Member and the overlying Tidwell Member.

Jurassic age appear to be affected by the Rocky Mesa faults, suggesting that the observed faults are confined to the Jurassic sandstones. As these were covered by a substantial thickness of Cretaceous and perhaps early Tertiary units at the time of faulting, fault development is inferred to have taken place at a moderate depth. All post-Jurassic units in the Rocky Mesa area were eroded away during Miocene uplift of the Colorado Plateau (Cater, 1970). The uppermost unit that can reasonably be deduced from outcrop data to have covered the Arches National Park area is the Cretaceous-aged Mancos Shale (Fig. 4), which crops out in Salt Valley. However, the Book Cliffs, 43 km north of Rocky Mesa, contain units as young as lower Tertiary Wasatch Formation (Willis, 1986) that were gently folded during the Laramide orogeny, analogous to the folding that produced the Moab Anticline. Doelling (1985, 1988) suggests that these units may have extended as far south as the Arches National Park vicinity. Using this reasoning, we calculated an overburden thickness at Rocky Mesa during active normal faulting that incorporates mid-Jurassic through early Tertiary stratigraphic units. This calculation indicates an approximate burial depth of 3.4 km at the vertical midpoint of the normal fault system, within the Navajo Sandstone.

2.3. Joint characteristics

A fault and joint map of the Rocky Mesa area (Fig. 7) illustrates that joint patterns are variable across the region of normal faulting. Focus in this study is given to a region where joints strike at high angles to normal faults near the northwestern end of the fault traces (Fig. 8). The joints are confined to inter-fault blocks and are not part of a regional set. Joints in nearby areas of the park (Garden Area, Devil's Garden, and Klondike Bluffs; Fig. 2), have a dominant NW trend essentially perpendicular to the joints shown in Fig. 8.

Joints terminate at the faults and the pattern of jointing is thus asymmetric from one side of a fault to the other (Fig. 8). Joints are distributed along fault surfaces with no direct indication as to whether growth was originally along the fault surface or at an old fault tipline location. In no instances are joints traceable across an exposed fault, indicating that joint growth occurred to one side of a fault surface or tip rather than ahead of a propagating fault tip, as has been documented for secondary structures along small strike-slip faults (Martel and Boger, 1998). Termination of joints against faults is most prevalent in the footwall block. Some joints breach the entire relay between overlapping faults, but the dominant trend is for joints to terminate before reaching the hanging wall surface of the adjacent fault bounding the relay.

There is little variation in the orientation and dip of the normal faults in the region where joints strike at high angles to faults. A fault is inferred to exist in the location of the dashed line in Fig. 8, on the basis of abrupt terminations in the map pattern of joints. A fault in this location defines an inter-fault block that confines the longest set of joints. There is no clearly identifiable fault at the surface in this location, although an increased deformation band density may indicate the upper extent of a fault below the surface, or the lower extent of a fault subsequently eroded away.

Joints extend throughout the thickness of the Moab

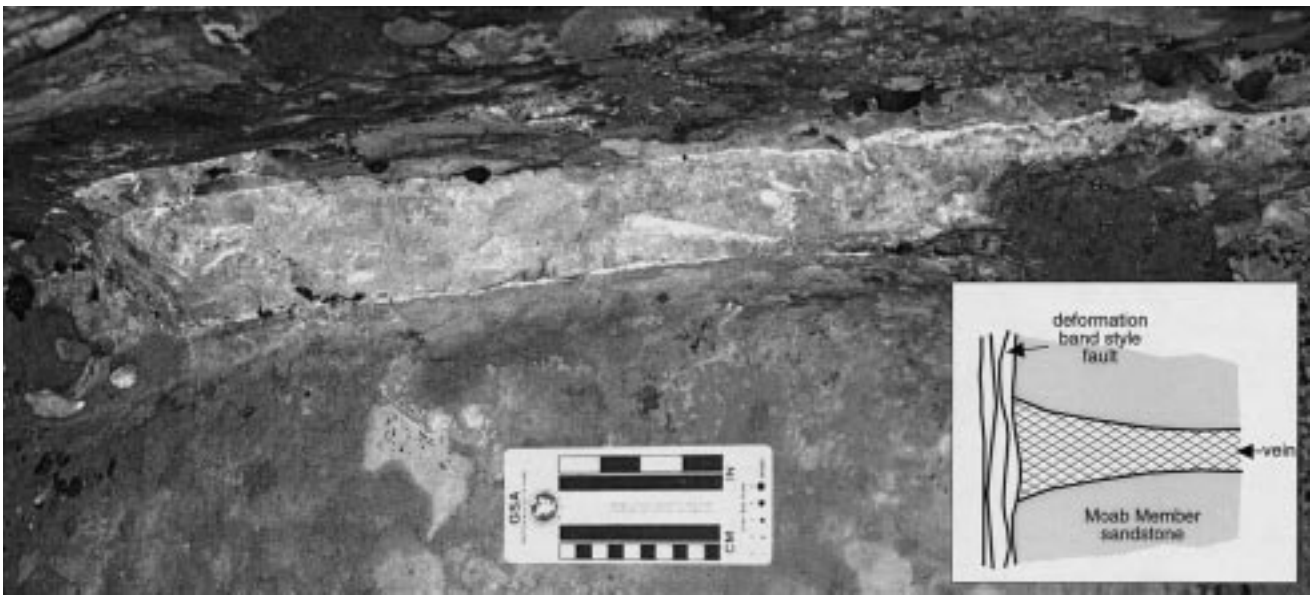

Fig. 9. A 7-cm-thick clay–calcite vein along a joint zone. The fault is to the left of the figure. Inset: vein geometry with respect to the fault. Veins occur in the footwall block and are thickest nearest the fault.

Member, and do not appear to continue into either the underlying Slick Rock Member of the Entrada Sandstone or the overlying Tidwell Member of the Morrison Formation. Individual joints exhibit straight outcrop traces (Fig. 8) and mutually adjacent joint segments do not appear to curve towards each other or intersect. The joints vary little in overall orientation and dip (Fig. 8 inset): they are predominantly within 20° of vertical, with a maximum deviation of 39° from vertical. Decreases in dip magnitude generally occur as joints approach the mechanical discontinuity that is the interface between the Moab Member and the overlying Tidwell Member (shale/limestone/chert). A similar effect has been observed near stratigraphic contacts elsewhere in Arches National Park (Cruikshank and Aydin, 1995). Some joints also display slight changes in orientation as they approach within a meter or so of the faults (Fig. 8).

Joint spacings are variable, although generally are between 10 and 30 m. This is comparable to the thickness of the Moab Member (~30 m), and may reflect documented observations of the approximate relationship between joint spacing and unit thickness (Price, 1966; Pollard and Segall, 1987). The density of joints is variable in the region away from the faults, whereas close to the faults and within narrow relay zones, joint density increases and is more consistent (Fig. 8; Kattenhorn, 1998). Joint densities decrease to zero in the uppermost meter or so of the Moab Member, reflecting the fact that the vertical extent of joints is limited and they do not intersect the contact with the overlying Tidwell Member.

Some joints were intruded by a fluidized clay to form veins (Fig. 9). From thin section analysis, the vein material is interpreted to be a clay and calcite cement supporting quartz grains seemingly fragmented away from the sandstone joint surfaces. Similar intrusive activity at Robert's Rift—a vertical fracture zone in Bull Canyon, 10 km west of Rocky Mesa (Hite, 1975)—has been attributed to the transport of brecciated material and fluids, derived from the Paradox Formation salt, up into fractured Jurassic sandstones. The timing of vein intrusion with respect to joint formation is uncertain. The veins either post-date the joints, having intruded along older fractures, possibly inducing new growth, or they are contemporaneous with initial joint growth. Episodic intrusion is suggested by veins-within-veins at one location. Veins occur immediately adjacent to fault footwalls at Rocky Mesa, suggesting faults acted as permeability barriers to migrating fluids, analogous to documented permeability decreases across deformation band-style faults elsewhere in Arches National Park (Antonellini and Aydin, 1995). If the veins were contemporaneous with joint growth, the difference between the fluid pressure and the least compressive remote stress (joint-perpendicular stress) was sufficient to overcome the fracture strength of the rock and promote joint propagation.

2.4. Sequence of fracturing

We used detailed observations of field relationships to determine the sequence of faulting and jointing at Rocky Mesa. Fault-parallel deformation bands are interpreted to be the genetic precursor to the develop-

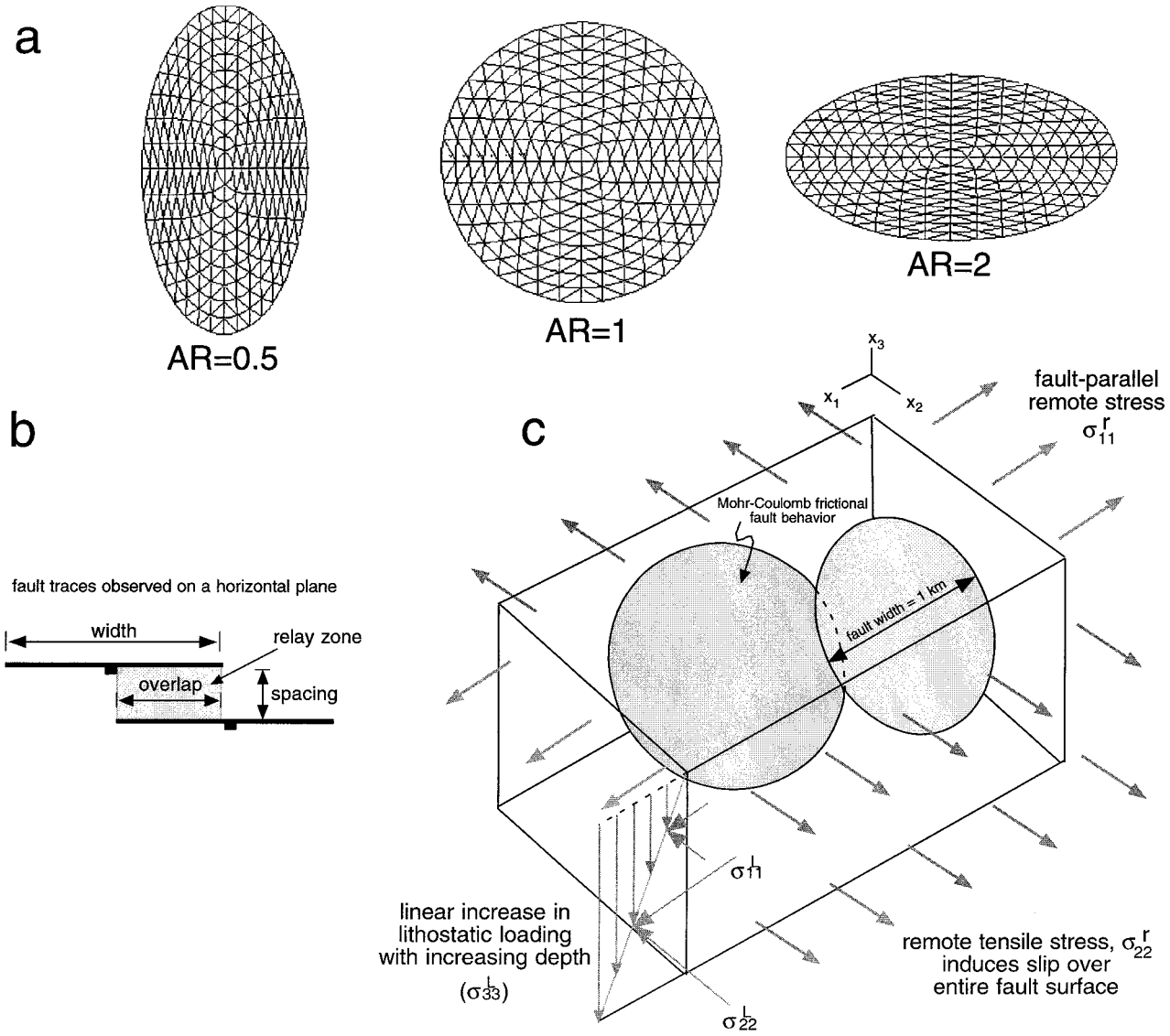

Fig. 10. (a) Discretized geometries of faults with variable aspect ratios (AR). (b) Map view of overlapping fault traces and associated terminologies. (c) Model configuration for overlapping faults in an infinite elastic body. Boundary conditions include a remote tectonic tension driving fault slip (σ^{r}_{22}), a fault-parallel remote tectonic stress (σ^{r}_{11}), and an increasing lithostatic load with increasing depth (σ^{L}_{ij}). The combined remote and lithostatic stresses produce a state of all-round compression in the vicinity of the faults.

ment of normal faults with slip surfaces. Fault-perpendicular joints cut (and are thus younger than) this deformation band set. The majority of joints have at least one end in map view connected to a fault slip surface. In no instances do joints cut through a fault to continue into the adjacent inter-fault block, indicating that faults are older and acted as mechanical barriers to joint growth.

Field evidence thus suggests that fault growth was accompanied by slip on discrete slip surfaces and joint development along the periphery of these surfaces where the stress fields were perturbed. Many, but not all, of the joints that formed along faults continued growing into the footwall blocks. Relay zone breach occurred between overlapping faults where joints propagated across the entire inter-fault block. Although some joints exhibit a change in orientation beyond a few meters of the faults (becoming almost fault-perpendicular), the absence of sudden, angular changes in joint orientation suggests a continuous stable episode of primary joint growth within a spatially or temporally variable stress field.

Tailcracks and horsetail fractures provide evidence that changes in the stress field *after* joint growth resolved sufficient shear on some joints to induce microslip (Cruikshank et al., 1991). Joints with strikes of ~025° show evidence of right-lateral shear whereas joints with strikes of ~045° underwent left-lateral

shear. The conflicting slip sense implies a maximum compression orientation of ~035°, essentially perpendicular to the normal faults at Rocky Mesa.

3. Numerical modeling

Field observations at Rocky Mesa are consistent with joint development being associated with faulting. We use numerical models to examine the stress field around idealized normal faults in order to investigate how joints might form in a fault-perturbed stress field. The 3-D numerical method addresses the effects of fault tipline shape and mechanical interaction of fault segments upon the numerical solution to the perturbed stress field. Using the underlying assumption that joints are opening mode cracks that form perpendicular to least compressive principal stresses of sufficient magnitude to break sandstone, we determine the locations and orientations of joints that might form as a consequence of fault slip.

3.1. Modeling method

We computed solutions to boundary value models of normal faults imbedded in an elastic whole-space using the program Poly3D (Thomas, 1993). Based upon the boundary element method (Crouch and Starfield, 1983; Becker, 1992), Poly3D incorporates the fundamental solution to an angular dislocation in a homogeneous, linear elastic half-space (Comninou and Dundurs, 1975; Jeyakumaran et al., 1992). A number of angular dislocations are juxtaposed to create polygonal boundary elements that collectively define discretized objects of arbitrary shape in three dimensions (Fig. 10a).

Boundary conditions in Poly3D can be applied remotely (as constant stresses or strains), at the centers of each element of the discretized crack surface (as tractions or displacements), or as combinations thereof. The program solves a series of linear algebraic equations that describe the influence on each element of every other element under a prescribed set of boundary conditions. Once the displacement distribution along a fault is determined, the static stress, strain and displacement fields around the fault are calculated using influence coefficient equations that relate the displacements at the fault to the resultant elastic field at any point in the surrounding linear elastic medium. This solution is superimposed upon the remote stress field boundary condition to produce the total elastic field. The governing equations implemented by Poly3D are described in Appendix A of Thomas (1993).

In order to elucidate the effect of 3-D fault shape and mechanical interaction of overlapping faults on the perturbed stress field, simple fault configurations were used in the models rather than a re-creation of the complex fault patterns observed in Arches National Park. Poly3D provides static solutions to the elastic field during a single slip event, or numerous superimposable slip events, but does not incorporate the effects of fault propagation or stress relaxation in the case of multiple slip events. The program thus cannot be used to recreate the sequence of events that led to the current fault geometries in the field. Instead, model solutions are used to characterize fault-related joint development at some stage in the fault growth history when a particular fault arrangement (e.g. a particular amount of overlap) existed. In reality, fault evolution through time would have resulted in numerous fault arrangements and joint growth episodes. The goal of the modeling is to demonstrate the nature of the perturbed stress field around: (1) isolated faults of variable aspect ratio (ratio of fault length to fault height; Fig. 10a); and (2) overlapping, mechanically interacting faults (Fig. 10b and c). In this way, we can demonstrate the range of orientations of joints that might develop in such perturbed stress fields. The conclusions based upon these simple models are then applied to observations at Rocky Mesa.

3.2. Model setup

The faults are restricted to elliptical tipline shapes and planar fault surfaces (Fig. 10). The tipline represents the fault termination, where displacement decreases to zero. Elliptical tiplines are an adequate approximation to some natural tipline shapes described in nature (Rippon, 1985; Barnett et al., 1987). The perturbed stress field varies along the tipline as a result of the variable mode of slip at different points (Germanovich et al., 1994; Martel and Boger, 1998), emphasizing the importance of a 3-D analysis.

Modeled faults were imbedded in an infinite elastic body, circumventing edge effects and effectively approximating the ~3.4-km burial depth estimated for the faults at Rocky Mesa. Free surface effects at this depth are negligible for faults having the dimensions of those at Rocky Mesa (Kattenhorn, 1998). The elastic properties of the body are consistent with measured values for sandstone (Bieniawski, 1984): density, $\rho = 2300\ \mathrm{kg/m^3}$; Poisson's ratio, $\nu = 0.25$; and elastic shear modulus, $G = 12$ GPa. All faults, irrespective of aspect ratio (AR), have a horizontal dimension (length) of 1 km with their centers at identical depths. In accordance with field measurements, all faults in the models were prescribed a dip of 50°. For the case of overlapping geometries, faults were not physically linked.

Each fault element was prescribed the condition of zero opening or interpenetration. Frictional resistance

to slip on the fault, the implementation of which is described by Kattenhorn (1998), accounts for the effect of an increasing lithostatic load along the fault surface in the down-dip direction (Fig. 10c). Fault slip is governed by a simple Coulomb frictional slip criterion, and is driven by a constant, remote tectonic tension applied perpendicular to fault strike, sufficient to promote slip over the entire fault surface. Maximum stress drops on modeled faults are approximately 5 MPa ($AR = 2$), 10 MPa ($AR = 1$) and 20 MPa ($AR = 0.5$), respectively. These values are within the range of calculated stress drops for natural normal fault seismic slip events (Mayeda and Walter, 1996).

We initially consider a state of stress before fault slip in which the vertical compression is equal to the fault-parallel compression. However, the component of stress parallel to the faults may be altered by tectonic contraction or extension, and may be less compressive than the vertical stress in response to a bilateral constraint (McGarr, 1988). For this reason, a fault-parallel stress component, σ^{r}_{11} (Fig. 10c), is subsequently incorporated into the static stress solution. A range of σ^{r}_{11} values are considered using the assumption that σ^{r}_{11} is less compressive than the vertical stress, σ^{r}_{33}. The σ^{r}_{11} remote stress component does not resolve onto the plane of the faults and therefore has no effect on fault slip.

The stress fields around slipped normal faults are described in subsequent sections as follows:

1. The characteristics of the perturbed field allow us to isolate the specific effect of this component of the total stress field on joint orientations very near the modeled faults.
2. The total stress field (perturbed + tectonic + lithostatic) is examined in order to demonstrate why the characteristics of the perturbed field alone are not sufficient to predict joint orientations.
3. The impact of variable ratios of fault-parallel to fault-perpendicular remote stresses on joint orientations is considered.

3.3. Characteristics of the perturbed field

The perturbation of the stress field is greatest near the tipline and secondary structures such as joints are most likely to initiate there. This observation is in agreement with crack growth at the tips of slipped interfaces described in field examples (Lajtai, 1969; Segall and Pollard, 1980; Martel et al., 1988; Cruikshank et al., 1991).

The nature of the perturbed field associated with a slip event on a frictional fault is shown in Fig. 11. These images exclude the remote stress field (tectonic and lithostatic components) in order to demonstrate the specific contribution of the perturbation by the faults to the final state of stress. The contour map of stress magnitudes on a horizontal plane intersecting the fault (Fig. 11b) exhibits an increase in stress magnitudes along the fault trace, particularly in the tipline vicinity. This pattern is consistent irrespective of the vertical position of the observation plane with respect to the fault. Superimposed on this image are the predicted orientations of joints that would result entirely as a consequence of the perturbed field. These potential joint planes were projected from 3-D space onto the horizontal plane of observation as strike lines (tick marks in Fig. 11b).

The perturbed field is variable near the tipline and the orientation of a secondary structure with respect to the fault thus depends entirely on the angular position (in the plane of observation) around the fault tip. Directly ahead of the tipline, in-plane with the fault surface, joints would form parallel to fault strike. This may provide a mechanism for fault propagation, with the development of numerous extension microcracks ahead of the tip that promote shear failure and fault elongation (Cox and Scholz, 1988; Anders and Wiltschko, 1994; Reches and Lockner, 1994). To either side of the fault tipline, joints may form along the fault surface at a variety of orientations, from fault-parallel to fault-perpendicular (Fig. 11b).

We calculated the maximum principal stress, σ_1 (tension positive), around several points along the tipline (Fig. 12, inset), from the top ($\theta = 90^{\circ}$) to the bottom ($\theta = -90^{\circ}$) of the fault, constraining the direction, Θ, around each point on the tipline that is most conducive to joint growth. These stresses were calculated from solutions to the stress tensor obtained using equations for the near-tip field (Lawn, 1993) of the form:

$$\sigma_{ij} = \frac{K}{(2\pi r)^{1/2}} f_{ij}(\Theta) \tag{1}$$

where K is the stress intensity factor for a given slip mode, r is radial distance from the tipline and Θ is the angular position around a point on the tipline.

Fig. 12 illustrates the normalized magnitudes of σ_1 around the tiplines of normal faults in 3-D for three fault aspect ratios, normalized to the maximum value for the $AR = 0.5$ case. Irrespective of fault aspect ratio, the maximum stress magnitudes are always at the upper tip, where the lithostatic confining stress is at a minimum. Solutions to Eq. (1) indicate that in the upper half of the fault, the maximum σ_1 occurs for $\Theta = -\pi$ (on the hanging wall surface of the fault) whereas in the lower half of the fault, the maximum σ_1 occurs for $\Theta = \pi$ (footwall surface of the fault; Fig. 12).

Furthermore, the maximum values of σ_1 occurring along the fault plane ($\Theta = \pm\pi$) are oriented in the

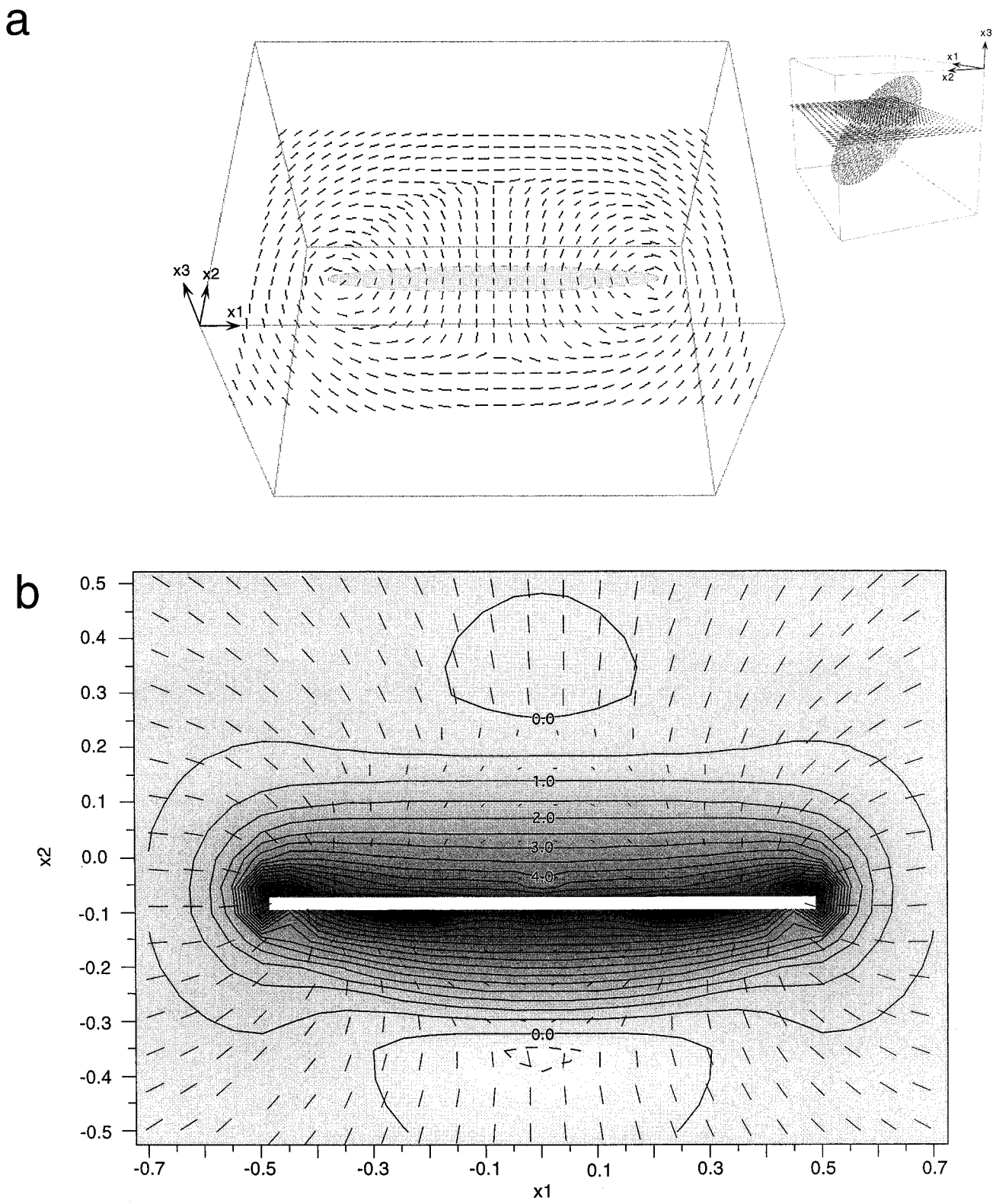

Fig. 11. (a) 3-D perspective view of the perturbed stress field around a circular normal fault along a horizontal observation plane a small distance above the fault center (inset). Tick marks represent the orientations of σ_1 in 3-D. (b) Contours of stress magnitudes (MPa) on the observation plane. The fault (white line) dips towards the positive x_2 direction. Maximum stresses are concentrated around the tipline in the hanging wall block. Tick marks represent the strikes of joints that would form in the perturbed field. Tick mark lengths represent joint dips. Longest ticks represent vertical joints (perpendicular to the observation plane).

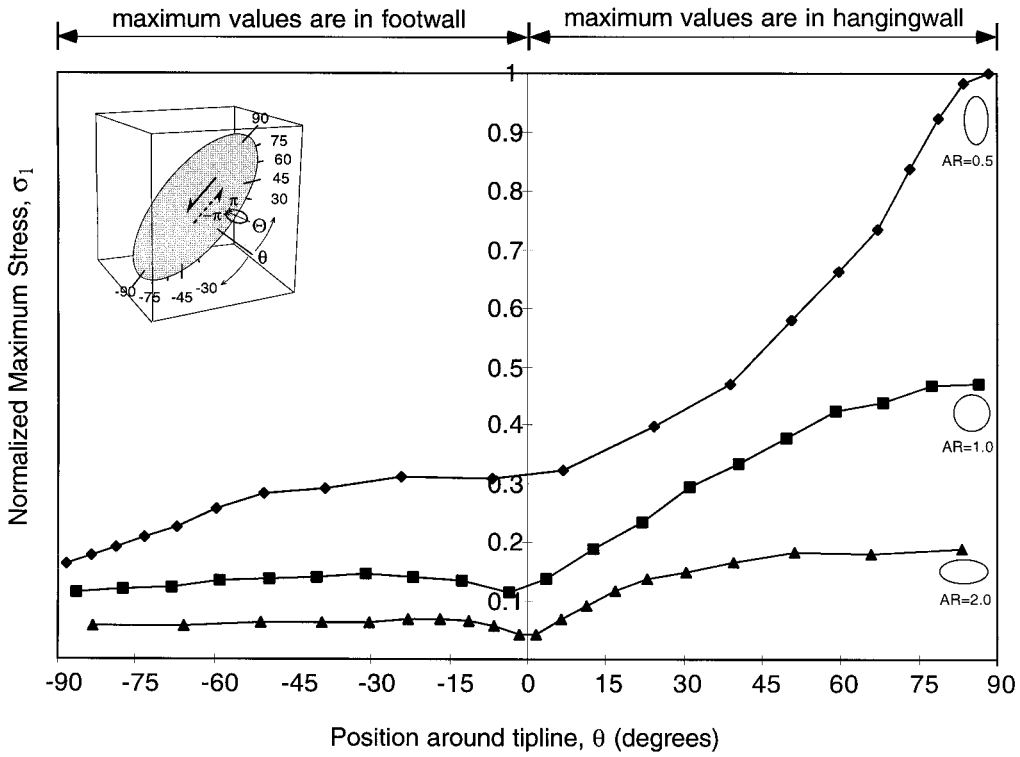

Fig. 12. Distributions of normalized maximum principal stress (σ_1) magnitudes around the tiplines of normal faults. Three aspect ratios are considered: $AR = 0.5$ (tall elliptical), 1.0 (circular) and 2.0 (wide elliptical). Position around the tipline, θ, shown on the inset figure. All magnitudes are normalized to the maximum value for the $AR = 0.5$ case. Maximum σ_1 values occur along the hanging wall surface ($\Theta = -\pi$) in the upper half of the fault and along the footwall surface ($\Theta = \pi$) in the lower half.

plane of the fault surface. All resultant joints are initiated perpendicular to the fault surface with normals perpendicular to the tipline. This results in joints that strike perpendicular to fault strike at the lateral fault tips but parallel to fault strike at the upper and lower tips. Thus, the orientations of joints with respect to the fault depend on the 3-D position along the fault tipline trace (Fig. 13a). Joints striking at high angles to faults are known from observations of secondary fractures at the lateral (mode II) tips of strike-slip faults. However, it is important to note that in this case, such a relationship is obtained in the absence of any strike-slip component of slip on the faults.

Joint orientations at the mode III tips in Fig. 13(a) differ from 2-D analytical models (Scholz, 1990), field observations of strike-slip faults (Martel and Boger, 1998), and experimental analyses of cracks in polymethyl methacrylate plastic (PMMA) (Adams and Sines, 1978; Cooke and Pollard, 1996) that predict échelon cracks ahead of a mode III crack tipline (Fig. 13b). The development and subsequent linkage of such fractures in rock may aid in growth of the shear plane at the mode III tip (Cox and Scholz, 1988). However, the model boundary conditions in this study, which incorporate the effect of increasing lithostatic stresses with depth on 3-D fault slip behavior, produce model results that predict maximum principal stress magnitudes along the fault plane instead of ahead of the tipline. Such behavior in nature may be aided by the presence of a cohesive zone towards a fault tip that induces an increased displacement gradient behind the tip and subsequent fracture growth along the fault plane (Cooke, 1997; Martel, 1997). Resultant secondary crack growth is to one side of the tipline only (Fig. 13a), as occurs at Rocky Mesa.

3.4. Characteristics of the total stress state

The orientations of secondary structures outside of the intensely perturbed field (e.g. beyond a few meters of a 1-km-long fault) are increasingly dependent on the remote state of stress rather than the perturbed field. For a stress state in which the lithostatic load is isotropic and fault slip is driven by a tensile tectonic stress acting perpendicular to fault strike (Fig. 10), σ_1 is parallel to the remote tectonic stress almost everywhere around a slipping normal fault (Fig. 14a and b). The observation points at which σ_1 is calculated are located 10 m perpendicularly away from the fault plane. Here, the remote field driving fault slip dominates over the perturbed field. Thus, any joints that are initiated and grow at distances of more than a few meters from the faults (~1% of the fault length) will have orientations dictated by the remote tensile stress.

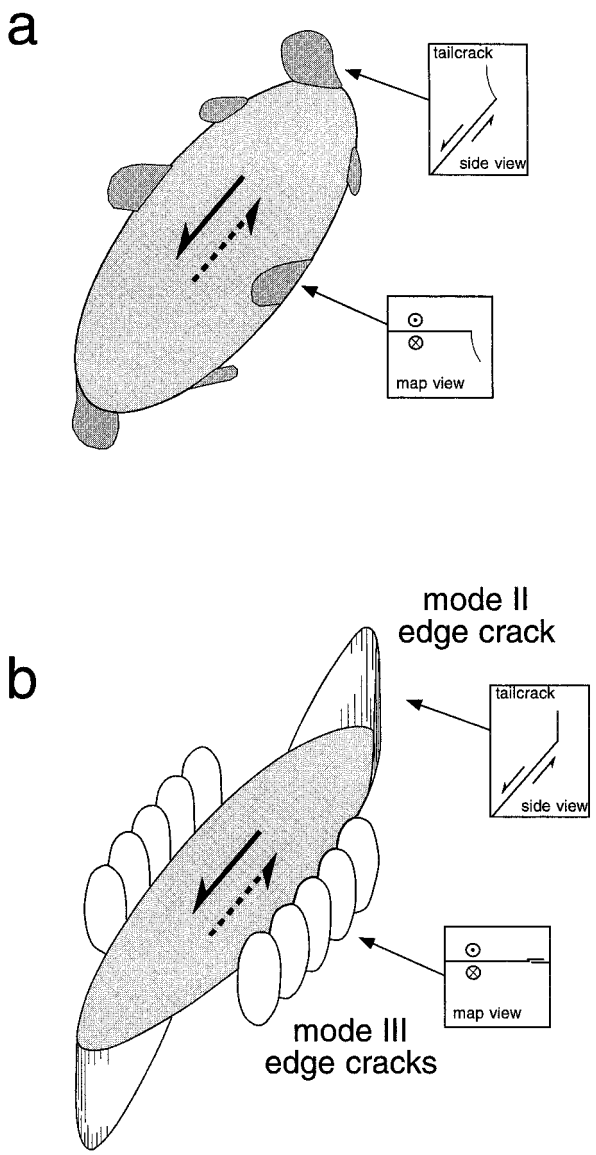

Fig. 13. Conceptual 3-D illustration of joint orientations along the tipline of an elliptical normal fault. At the top of the fault, joints in section view resemble tailcracks seen along strike-slip faults in map view. Such joints have strike orientations parallel to normal faults in map view. Along the lateral edges of the tipline, joints may grow away from the fault plane at high angles to fault strike. (b) Conventional idea of edge cracks around a slipping fault (Scholz, 1990). Échelon cracks form ahead of the lateral fault tips.

Such joints would therefore be vertical and oriented parallel to fault strike.

However, in the absence of high pore pressures, tensile stresses that exceed the fracture strength of the rock at depth may only occur in the perturbed field very close to the fault plane. Joints initiating in this field at the upper fault tip, where hanging wall tensile stresses are greatest, would be initiated at an angle to the fault plane (but with identical strike orientations), then would steepen away from the fault as they propagate into the region dominated by the remote field (Fig. 13a). In locations along the fault tipline where joints are initiated at high angles to fault strike, the remote field impedes joint propagation into the surrounding rock because σ_1 rotates into parallelism with joint strike within a few meters of the fault (Fig. 14). In such a state of stress, joints at high angles to faults should be short and restricted to the near-fault region. Any additional growth, such as under the driving stress of high internal fluid pressures in the joints, would result in large curvatures in joint strikes as the joints propagate into the dominant remote stress field.

For discontinuous fault geometries, where individual fault segments overlap and mechanically interact, the greatest perturbation effect occurs within the relay zone between the faults. However, perturbed field σ_1 orientations within the relay are only slightly rotated with respect to the remote field (Fig. 15). This is the case for all amounts of overlap (fault spacing is kept constant at 50 m, or 5% of the fault length), although the rotation of σ_1 with respect to the remote field increases as fault aspect ratio decreases (faults get taller). Wide elliptical faults ($AR = 2$) have no noticeable perturbation across the relay. This is attributable to the fault height effect wherein tall elliptical faults perturb the stress field to a greater distance away from the fault than wide elliptical faults (Willemse et al., 1996).

3.5. Effect of remote horizontal stress ratio

In order to consider a range of plausible remote stress conditions, we evaluated the effect of the fault-parallel stress on the orientation of principal stress axes around overlapping normal faults. This was accomplished by including a fault-parallel remote stress component, σ^{r}_{11}, in the model boundary conditions (Fig. 10c). The fault-parallel stress component may address a variety of crustal conditions: fault-parallel bending stresses (e.g. in doubly-plunging anticlines—possibly the case for the Moab Anticline), the lithostatic bilateral constraint effect (McGarr, 1988), remote tectonic tensile stresses, or a rotation of the maximum tension from fault-perpendicular to fault-parallel due to relaxation of the initial fault-perpendicular σ^{r}_{22} by extensional faulting.

We introduce a variable, δ, to represent the *remote horizontal stress ratio*: the ratio of fault-parallel to fault-perpendicular remote stress ($\sigma^{r}_{11}/\sigma^{r}_{22}$). In order to address fault and joint configurations such as those observed at Rocky Mesa in Arches National Park, we calculated orientations of σ_1 at observation points 10 m away from overlapping faults for various values of δ (Fig. 16). The associated principal stress conditions for each δ, as would occur at any arbitrary point on the fault, are shown in Fig. 17. The most noticeable effect in Fig. 16 is an increasing rotation of

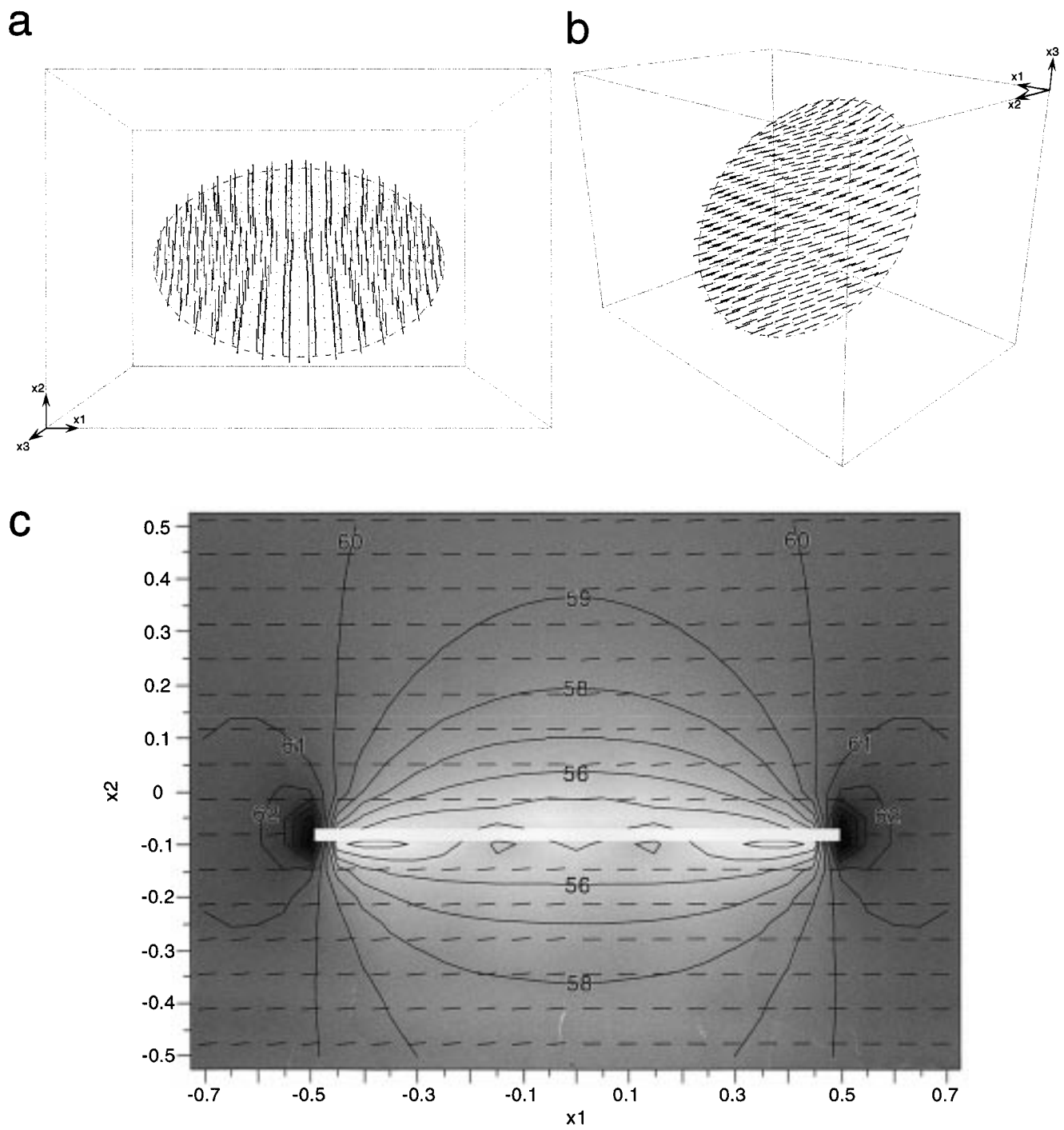

Fig. 14. (a) Orientations of maximum principal stress trajectories for a state of stress that includes the remote and perturbed stress field components. Observation points are 10 m away from the fault plane in the hanging wall. View is from directly above. Trajectories are generally aligned with the remote tectonic stress field (x_2 direction). (b) Oblique perspective view. (c) Contours of stress magnitudes (in MPa) and strikes of joints that would form in the total stress field (compare to Fig. 11b). Joints are aligned parallel to fault strike. Highest stress magnitudes are around the fault tipline whereas lowest stresses are along the fault plane away from the tipline.

σ_1 in the relay zone with respect to the remote field as δ increases. The relay zone perturbation of the stress field by the faults is thus increasingly enhanced with increasing δ. Outside of the relay zone, the magnitude of δ has little effect on the stress field around the faults (except along the tipline) because σ_{22}^{r} remains the dominant control on local σ_1 orientations. Only when $\delta > 1$ does σ_1 become sub-parallel to fault strike at

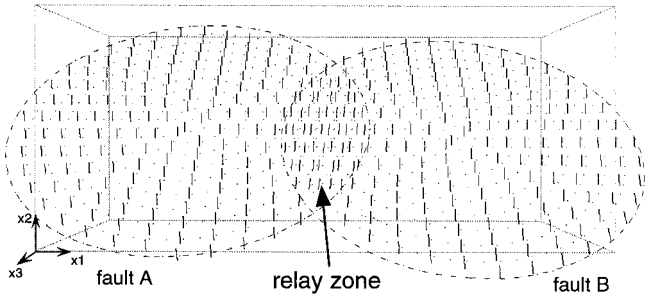

Fig. 15. Maximum principal stresses for overlapping circular faults subject to a uniaxial tension (25% overlap, 5% spacing; view from directly above; faults dip in positive x_2 direction). The perturbed field is overprinted by the remote field. A slight perturbation effect extends across the relay zone between the faults. Observation points are 10 m into the footwall block of fault A and 10 m into the hanging wall block of fault B.

most observation points. This condition is unlikely to occur during the initiation of faults because normal faults develop with their strikes perpendicular to the direction of maximum tensile stress. For $\delta > 1$, fault orientations should thus be perpendicular to the orientation of the faults in our models. However, existing faults (which may form zones of weakness compared to intact rock) can continue to accumulate slip after a rotation of the principal stress axes. This may occur despite the fact that the faults no longer strike perpendicular to the remote maximum principal tensile stress.

Irrespective of the specific controls on the value of δ during the evolution of a normal fault, the results in Fig. 16 indicate that for homogeneous rocks, the remote horizontal stress ratio in normal faulting environments plays perhaps the most dominant role in controlling the orientations of secondary structures developing in the relay zone between overlapping, planar normal faults.

4. Discussion

Detailed field observations indicate that joints striking at high angles to normal faults at Rocky Mesa are related to the faulting. The state of stress during joint growth included fault-perpendicular tension induced by bending, lithostatic stresses, perturbation of the stress field by normal fault slip, regional tectonic stresses during and subsequent to the Laramide orogeny, and possibly internal fluid pressures in joints. Any hypothesis for the history of joint growth should reconcile this state of stress with field characteristics of the fault and joint system.

We have described numerical model results that demonstrate the perturbation of the stress field during slip along normal faults. The perturbed field may produce a range of joint orientations and joint patterns near to both isolated and mechanically interacting faults. Calculated maximum principal stresses along the model fault tiplines indicate that joints can grow at high angles to fault strike near the lateral tips. This provides a mechanical rationale from which we infer that joints striking at high angles to normal faults at Rocky Mesa may have formed along propagating lateral fault tips.

Numerical model results suggest that joints propagating across a normal fault relay zone under conditions of a remote tectonic tension and an isotropic lithostatic stress (Fig. 15) will be oriented at a shallow, oblique angle to fault strike. For a given overlap, this angle is greatest for tall faults ($AR < 1$) and does not exceed about 30°. In contrast, at Rocky Mesa, where the overlapping fault segment geometries are similar to the numerical models, the angle between fault strike and joint strike is approximately 75°, and the faults appear to be wide with aspect ratios between 1 and 4.

Furthermore, the perturbed field in each model (Fig. 11) is overprinted by the effect of the remote field (Fig. 14) within a few meters of 1-km-long faults. The perturbation effect extends furthest from faults near the fault tipline, where the sudden loss of slip results in high stress magnitudes (greatest at the upper tip of the fault, decreasing to the bottom tip), and within relay zones between overlapping faults. At Rocky Mesa, joints extend up to 400 m away from faults that are at most 4 km long. This distance of 10% of the fault length for perturbed field predominance is not substantiated by numerical models in which the fault-parallel stress consists solely of the isotropic lithostatic load (Fig. 15).

However, numerical models that incorporate an intermediate remote principal stress acting parallel to normal fault strike that is different from an isotropic lithostatic stress value (Fig. 16) produce results that allow joint growth for significant distances away from, and at high angles to, the faults. The ratio of fault-parallel to fault-perpendicular remote stress, δ, may vary with tectonic setting and may undergo temporal variations during and after faulting. For $\delta < 0.5$, the orientations of principal stresses in a relay zone are predominantly controlled by the maximum remote principal stress acting perpendicular to fault strike. Thus, relay-breaching joints would not form at high angles to fault strike. As δ increases ($\delta > 0.5$), rotations of σ_1 within the relay zone promote continued propagation of joints forming at high angles to fault strike in the perturbed stress field, such as occurred at Rocky Mesa.

It is important, therefore, to establish whether or not the fault-parallel remote stress at Rocky Mesa approached or perhaps eventually exceeded the initial fault-perpendicular remote stress responsible for fault initiation and growth, resulting in an increased δ

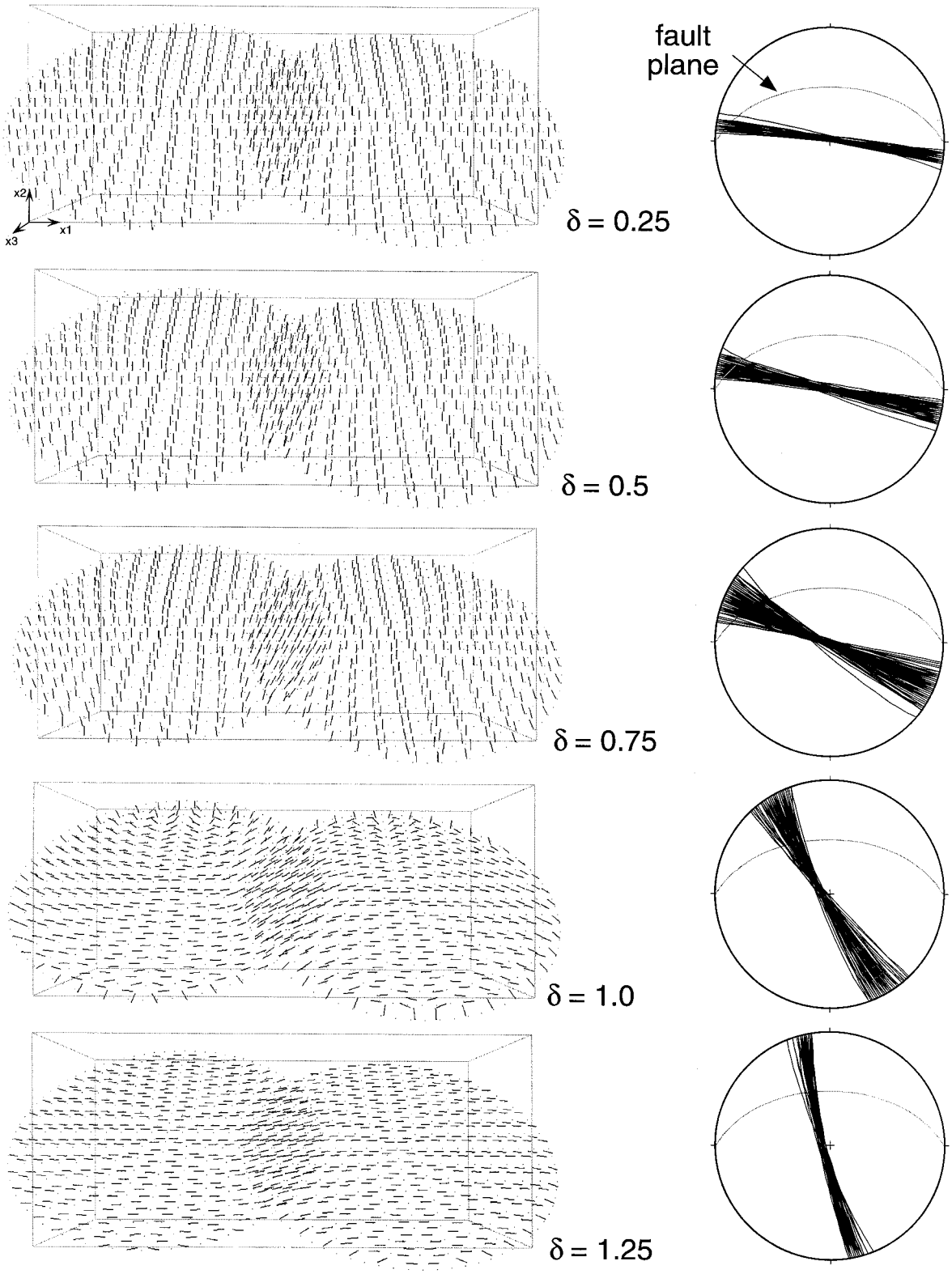

Fig. 16. Effect of the horizontal stress ratio, δ (ratio of fault-parallel to fault-perpendicular remote stress) on perturbed maximum principal stress orientations near overlapping circular normal faults. View is from directly above the faults. Observation point locations are as in Fig. 15. Relay zone stresses are particularly sensitive to δ. Numerical predictions of joint orientations in relay zones are plotted on stereonets ($n = 114$; grey circles are faults).

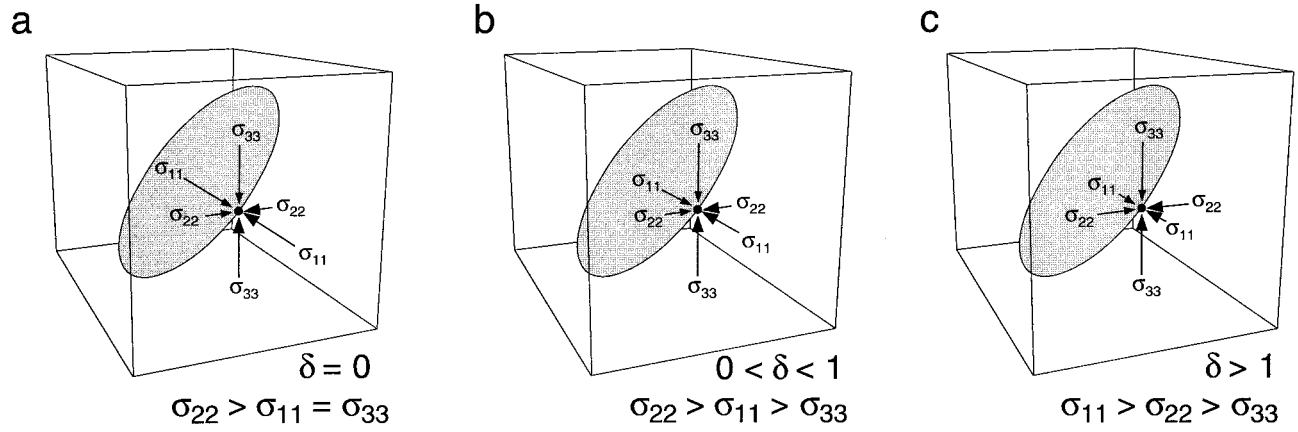

Fig. 17. Relative principal stress boundary conditions at *any* arbitrary point on a fault plane for various values of the remote horizontal stress ratio, δ. (a) For $\delta = 0$, a uniaxial remote tension is applied perpendicular to fault strike. The fault-parallel stress is equal to the lithostatic load. (b) For δ between 0 and 1, the fault-parallel stress is greater (more tensile) than the lithostatic load but less than the fault-perpendicular stress. (c) When $\delta > 1$, the maximum tension has rotated parallel to fault strike.

during or immediately after fault slip. Occurrences of stress field rotations in regions of extension have been reported from grabens in Iceland (Price and Cosgrove, 1990, p. 186) and have been attributed to the formation of orthogonal joint patterns in nature and laboratory experiments (Rives et al., 1994). In the context of Rocky Mesa, the maximum principal stress perpendicular to fault strike is interpreted to have been induced by bending of the rock units during the Laramide orogeny. It is possible that faulting and deformation band growth along the crest of the Moab Anticline caused relatively rapid (in a geologic sense) cyclic decreases in the fault-perpendicular maximum local principal stress (i.e. increased compression) to values less than the original fault-parallel intermediate local principal stress.

The rationale for this hypothesis is that bending was greatly influenced by activity along the Moab Fault, so that variations in bending stresses would have been directly linked to Moab Fault activity. In periods of quiescence along the Moab Fault, relaxation of local fault-perpendicular stresses by normal faults at Rocky Mesa may have resulted in a relative increase in the fault-parallel stress. Such occurrences of local stress rotation may have been accentuated by the northeast-directed compressive Laramide remote tectonic stress acting perpendicular to fault strike. If the faults continued to accumulate slip in this new stress state ($\delta > 1$; Fig. 17c), predicted joint orientations are at high angles to fault strike everywhere outside of the perturbed field influence, approaching the geometry observed at Rocky Mesa when $\delta \approx 1.25$ (Fig. 16).

Under such stress conditions, joints forming at high angles to fault strike along the tipline and in relay zones would have been able to propagate a significant distance from the fault. Although speculative, fluid pressures within joints may have contributed to the driving stress for joint propagation, as suggested by the vein intrusion of joints at Rocky Mesa. In addition, stress conditions would have been favorable for new growth of short, fault-perpendicular joints abandoned along the fault surface behind the propagating tipline. Growth of joints in this manner generally results in a self-similar organization of joints (Nemat-Nasser et al., 1979) with a characteristic spacing related to unit thickness (Pollard and Segall, 1987), as appears to be the case at Rocky Mesa. A final line of evidence for the stress rotations at Rocky Mesa is provided by tailcracks along some of the joints. These cracks indicate that a compressive stress acting perpendicular to fault strike resolved sufficient shear on existing joints to induce microslip.

In summary, the sequence of events at Rocky Mesa began with the development of the Moab Anticline during the Laramide tectonic event. Bending along a NW–SE axis was accentuated by recurrent activity along the Moab Fault. Strain was accommodated along the anticline axis through the development of deformation bands which subsequently evolved into normal faults. Slip along the faults perturbed the local stress fields and resulted in the simultaneous development of joints adjacent to the faults. Joints formed at approximately 75° to fault strike, indicating that the fault-parallel stress became similar to the fault-perpendicular stress during joint growth. This may have resulted from a combination of temporal variations in the relaxation of fault-perpendicular bending stresses across the anticline associated with fault slip events, and Laramide remote compressive stresses acting perpendicular to faults. This process may have occurred repeatedly as the faults grew, resulting in a succession of joint growth episodes as the faults propagated laterally. As a result, joints occur along the length of the fault trace, each representing a growth episode at the

lateral fault tip before the tip advanced further into unfaulted rock, abandoning the joints behind it. The exact number of faulting and jointing events cannot be quantified in the absence of determinable tip propagation directions at each point along the fault trace or the number of joints that form per slip event.

Although the above discussion focuses on the growth of joints at high angles to normal fault strike, numerical model results indicate that fault-perturbed stresses can produce joints in a variety of orientations depending on the location along the fault tipline. Joints that form at the upper fault tip are parallel to fault strike in map view (Fig. 13). Considering that the upper tip is the region of highest stress along the tipline, fault-parallel joints may be the most probable to occur along normal faults contained wholly in the Earth's crust. Martel and Boger (1998) propose a similar variability in the probability of joint growth related to variations in stress magnitudes around the peripheries of strike-slip faults.

The two examples of fault and joint relationships in Fig. 1 may be thought of as end-members in a range of possible joint orientations around slipping normal faults and a degree of variability in relative fault and joint orientations should be expected in nature. For example, near the entrance to Arches National Park (Fig. 7), a fanning pattern of joints emanates away from a segment of the Moab Fault. The map pattern of the joints is very similar to that predicted by the perturbed field maximum principal stress orientations around the lateral tips of normal faults in numerical models (Fig. 11).

It should be noted that where normal faults develop with orientations described by Anderson (1951), the orientation of joints in the fault environment is also dependent upon timing. If joint growth precedes faulting, joints should form perpendicular to the maximum tensile remote principal stress. Subsequent normal faults would have similar strikes to the joints. However, if normal fault development precedes joint growth, perturbation of the stress field by the faults may result in joints that range from fault-parallel to fault-perpendicular.

We may perhaps apply these results to environments where the orientations of joints associated with faulting below the Earth's surface are not directly measurable. Vein infill material in the joints at Rocky Mesa is consistently restricted to the footwall side of faults, suggesting local compartmentalization of fluid flow by the faults. Many of the world's oilfields are compartmentalized by normal faults (e.g. Ottesen Ellevset et al., 1998), commonly resulting from the overlap and linkage of initially separate segments. A knowledge of joint orientations around segmented faults in the subsurface is crucial to the characterization of fracture permeability within a reservoir. Increasingly accurate fault geometry characterization is now possible through 3-D seismic survey interpretations (Kattenhorn, 1998). Measurements of the *in situ* stress state in the reservoir may be combined with interpreted fault geometries to numerically predict likely locations and orientations of joints in a reservoir. Although such predictions need to be tested through other means, such as borehole analyses of natural fracture orientations and geophysical methods, the results described here provide a starting point for such predictive tools.

Another application of our model results pertains to the nature of fault segment linkage in normal fault systems. The development of joints at high angles to normal faults in relays may result in hard linkage of adjacent fault segments before significant overlap can be achieved. Martel and Boger (1998) indicate that lateral linkage of strike-slip faults is promoted by the growth of tailcracks where the fault tipline slips in mode II, and that normal faults are more likely to form vertical linkage points where similar secondary cracks develop at the upper and lower fault tips. However, this prediction contrasts with documented high fault aspect ratios (wide faults) for both normal and strike-slip faults (Nicol et al., 1996). High aspect ratios for normal faults have been attributed to the effect of mechanical anisotropy in layered sedimentary rocks (Mansfield and Cartwright, 1996; Martel and Boger, 1998; Kattenhorn, 1999). This study, however, provides an alternative mechanism for the lateral linkage of normal fault segments through relay breaching by joints, resulting in increases in composite fault aspect ratios. Transfer of slip along hard linkage features (joints) at high angles to normal faults have been described in natural normal fault systems (Trudgill and Cartwright, 1994; Cartwright and Mansfield, 1998). However, if the state of stress around normal faults is only conducive to the development of fractures at low angles to fault strike, then hard linkage of adjacent fault segments may not occur, or may occur only for high values of the fault overlap-to-spacing ratio.

5. Conclusions

Observations of normal fault and joint relationships in Arches National Park imply a genetic relationship between faulting and resultant joint development at high angles to fault strike. A numerical analysis of stress fields around normal faults at depth indicates that slip events perturb the stress field in the near-tip region ($<1\%$ of the fault length) in a complex and highly variable manner. At the upper tips of faults, high stress magnitudes result in joints that form with identical strikes to the faults, similar to the predictions

of Anderson (1951). Closer to the lateral tiplines, joints may form approximately perpendicular to normal faults. However, the lengths of such joints are dependent on the remote stress state. Away from the near-tip region the remote stress field orientation dominates so that faulting by uniaxial extension favors joint growth parallel to faults. In regions of fault overlap joint growth can occur oblique to faults, but rotations of the maximum principal stresses in the relay zone with respect to the remote tectonic stress are small ($< 30^\circ$).

However, the state of stress within a relay zone can be strongly affected by the remote stress acting parallel to fault strike. The ratio of fault-parallel to fault-perpendicular remote stresses, δ, is a major contributor to the orientations of joints, particularly in relay zones. As the remote fault-parallel stress magnitude increases with respect to the fault-perpendicular stress, the angle between faults and relay joints also increases.

The numerical model results and observations at Arches National Park allow an internally consistent hypothesis for joint development. At some time during the slip history of normal faults at Rough and Rocky Mesa, the fault-parallel remote stress approached and perhaps exceeded the fault-perpendicular stress that originally induced faulting. The resultant high value of δ, combined with perturbation effects induced by fault tipline shape and the geometric arrangement of overlapping faults, promoted the growth of joints at high angles ($\sim 75^\circ$) to fault strike. These observations complement predictions of mode I fracturing parallel to fault strike (Anderson, 1951) by demonstrating that joints in a normal faulting environment may also form with strike orientations almost perpendicular to faults.

Acknowledgements

Funding was provided by the U.S. Department of Energy, Grant No. DEFG03-94ER14462, and the Rock Fracture Project of Stanford University. We benefited from insightful discussions with Juliet Crider, Michele Cooke, Manuel Willemse, and Laurent Maerten. Sincere thanks to Thomas Roznovsky for providing assistance with field mapping. We acknowledge the National Park Service for their support of scientific research in the parks, particularly Karen McKinlay-Jones at Arches National Park. Finally, we are grateful to Bruce Trudgill and Jonathan Caine for their careful reviews that enabled us to improve upon our original manuscript.

References

Adams, M., Sines, G., 1978. Crack extension from flaws in a brittle material subject to compression. Tectonophysics 49, 97–118.

Anders, M.H., Wiltschko, D.V., 1994. Microfracturing, paleostress and the growth of faults. Journal of Structural Geology 16, 795–815.

Anderson, E.M., 1951. The Dynamics of Faulting. Oliver & Boyd, Edinburgh.

Antonellini, M., Aydin, A., 1994. Effect of faulting on fluid flow in porous sandstones: petrophysical properties. American Association of Petroleum Geologists Bulletin 78, 355–377.

Antonellini, M., Aydin, A., 1995. Effect of faulting on fluid flow in porous sandstones: geometry and spatial distribution. American Association of Petroleum Geologists Bulletin 79, 642–671.

Antonellini, M.A., Aydin, A., Pollard, D.D., 1994a. Microstructure of deformation bands in porous sandstones at Arches National Park, Utah. Journal of Structural Geology 16, 941–959.

Antonellini, M., Aydin, A., Pollard, D.D., D'Onfro, P., 1994b. Petrophysical study of faults in sandstone using petrographic image analysis and X-ray computerized tomography. Pure and Applied Geophysics 143, 181–201.

Aydin, A., Johnson, A.M., 1978. Development of faults as zones of deformation bands and as slip surfaces in sandstone. Pure and Applied Geophysics 116, 931–942.

Aydin, A., 1978. Small faults formed as deformation bands in sandstone. Pure and Applied Geophysics 116, 913–930.

Baars, D.L., Doelling, H.H., 1987. Moab salt-intruded anticline, east-central Utah. Geological Society of America Centennial Field Guide—Rocky Mountain Section, pp. 275–280.

Baars, D.L., Stevenson, G.M., 1981. Tectonic evolution of the Paradox Basin, Utah and Colorado. In: Wiegand, D.L. (Ed.), Geology of the Paradox Basin. Rocky Mountain Association of Geologists, pp. 23–31.

Baer, G., Reches, Z., 1991. Mechanics of emplacement and tectonic implications of the Ramon Dike Systems, Israel. Journal of Geophysical Research 96, 11895–11910.

Barnett, J.M., Mortimer, J., Rippon, J., Walsh, J.J., Watterson, J., 1987. Displacement geometry in the volume containing a single normal fault. American Association of Petroleum Geologists Bulletin 71, 925–937.

Barton, C.A., Zoback, M.D., 1994. Stress perturbations associated with active faults penetrated by boreholes: Possible evidence for near-complete stress drop and a new technique for stress magnitude measurement. Journal of Geophysical Research 99, 9373–9390.

Becker, A.A., 1992. The Boundary Element Method in Engineering. McGraw-Hill, New York.

Bieniawski, Z.T., 1984. Rock Mechanics Design in Mining and Tunneling. A.A. Balkema, Rotterdam.

Bürgmann, R., Pollard, D.D., Martel, S.J., 1994. Slip distributions on faults: effects of stress gradients, inelastic deformation, heterogeneous host-rock stiffness, and fault interaction. Journal of Structural Geology 16, 1675–1690.

Cartwright, J.A., Mansfield, C.S., 1998. Lateral displacement variation and lateral tip geometry of normal faults in the Canyonlands National Park, Utah. Journal of Structural Geology 20, 3–19.

Cater, F.W., 1970. Geology of the salt anticline region in southwestern Colorado. United States Geological Survey Professional Paper 637.

Comninou, M.A., Dundurs, J., 1975. The angular dislocation in a half-space. Journal of Elasticity 5, 203–216.

Cooke, M.L., Pollard, D.D., 1996. Fracture propagation paths under mixed mode loading within rectangular blocks of polymethyl methacrylate. Journal of Geophysical Research 101, 3387–3400.

Cooke, M.L., 1997. Fracture localization along faults with spatially varying friction. Journal of Geophysical Research 102, 22425–22434.

Cox, S.J.D., Scholz, C.H., 1988. On the formation and growth of

faults: an experimental study. Journal of Structural Geology 10, 413–430.
Crouch, S.L., Starfield, A.M., 1983. Boundary Element Methods in Solid Mechanics. Unwin Hyman, London.
Cruikshank, K.M., Aydin, A., 1994. Role of fracture localization in arch formation, Arches National Park, Utah. Geological Society of America Bulletin 106, 879–891.
Cruikshank, K.M., Aydin, A., 1995. Unweaving the joints in Entrada Sandstone, Arches National Park, Utah, U.S.A. Journal of Structural Geology 17, 409–421.
Cruikshank, K.M., Zhao, G., Johnson, A.M., 1991. Analysis of minor fractures associated with joints and faulted joints. Journal of Structural Geology 13, 865–886.
Delaney, P.T., Pollard, D.D., 1981. Deformation of host rocks and flow of magma during growth of minette dikes and breccia-bearing intrusions near Ship Rock, New Mexico. United States Geological Survey Professional Paper 1202.
Delaney, P.T., Pollard, D.D., Ziony, J.I., McKee, E.H., 1986. Field relations between dikes and joints: emplacement processes and paleostress analysis. Journal of Geophysical Research 91, 4920–4938.
Doelling, H.H., Yonkee, W.A., Hand, J.S., 1994. Geologic map of the Gold Bar Canyon quadrangle, Grand County, Utah. Utah Geological Survey Map 155, scale 1:24,000.
Doelling, H.H., Ross, M.L., Mulvey, W.E., 1995. Interim geologic map of the Moab quadrangle, Grand County, Utah. Utah Geological Survey Open-File Report 322.
Doelling, H.H., 1985. Geology of Arches National Park. Utah Geological and Mineral Survey Map 74, scale 1:50,000.
Doelling, H.H., 1988. Geology of Salt Valley Anticline and Arches National Park, Grand County, Utah. In: Doelling, H.H., Oviatt, C.G., Huntoon, P.W. (Eds.), Salt Deformation in the Paradox Region. Utah Geological and Mineral Survey Bulletin 122, pp. 3–58.
Dyer, J.R., 1983. Jointing in sandstones, Arches National Park, Utah. PhD thesis, Stanford University.
Dyer, R., 1988. Using joint interactions to estimate paleostress ratios. Journal of Structural Geology 10, 685–699.
Foxford, K.A., Garden, I.R., Guscott, S.C., Burley, S.D., Lewis, J.J.M., Walsh, J.J., Watterson, J., 1996. The field geology of the Moab Fault. In: Huffman Jr, A.C., Lund, W.R., Godwin, L.H. (Eds.), Geology and Resources of the Paradox Basin. Utah Geological Association Guidebook 25, pp. 265–283.
Friedman, J.D., Case, J.E., Simpson, S.L., 1994. Tectonic trends of the northern part of the Paradox Basin, southeastern Utah and southwestern Colorado, as derived from Landsat multispectral scanner imaging and geophysical and geological mapping. United States Geological Survey Bulletin 2000-C.
Gard, L.M.J., 1976. Geology of the north end of the Salt Valley anticline, Grand County, Utah. United States Geological Survey Open-File Report 76-303.
Germanovich, L.N., Salganik, R.L., Dyskin, A.V., Lee, K.K., 1994. Mechanisms of brittle fracture of rock with pre-existing cracks in compression. Pure and Applied Geophysics 143, 117–149.
Hecker, S., 1993. Quaternary tectonics of Utah with emphasis on earthquake-hazard characterization. Utah Geological Survey Bulletin 127.
Hite, R.J., 1975. An unusual northeast-trending fracture zone and its relations to basement wrench faulting in northern Paradox Basin, Utah and Colorado. Four Corners Geological Society Guidebook, 8th Field Conference, pp. 217–224.
Homberg, C., Hu, J.C., Angelier, J., Bergerat, F., Lacombe, O., 1997. Characterization of stress perturbations near major fault zones: insights from 2-D distinct-element numerical modelling and field studies (Jura mountains). Journal of Structural Geology 19, 703–718.
Huntoon, P.W., 1982. The Meander anticline, Canyonlands, Utah: An unloading structure resulting from horizontal gliding of salt. Geological Society of America Bulletin 93, 941–950.
Huntoon, P.W., 1988. Late Cenozoic gravity tectonic deformation related to the Paradox salts in the Canyonlands area of Utah. In: Doelling, H.H., Oviatt, C.G., Huntoon, P.W. (Eds.), Salt Deformation in the Paradox Region. Utah Geological and Mineral Survey Bulletin 122, pp. 81–93.
Jeyakumaran, M., Rudnicki, J.W., Keer, L.M., 1992. Modeling slip zones with triangular dislocation elements. Bulletin of the Seismological Society of America 82, 2153–2169.
Kattenhorn, S.A., Watkeys, M.K., 1995. Blunt-ended dyke segments. Journal of Structural Geology 17, 1535–1542.
Kattenhorn, S.A., 1998. A 3D mechanical analysis of normal fault evolution and joint development in perturbed stress fields around normal faults. PhD thesis, Stanford University.
Kattenhorn, S.A., 1999. Characteristics and evolution of segmented normal faults in 3-D. Eos, Transactions of the American Geophysical Union 80 (17), S328.
Lajtai, E.Z., 1969. Mechanics of second order faults and tension gashes. Geological Society of America Bulletin 80, 2253–2272.
Lawn, B., 1993. Fracture of Brittle Solids, 2nd ed. Cambridge University Press, Cambridge.
Mansfield, C.S., Cartwright, J.A., 1996. High resolution fault displacement mapping from three-dimensional seismic data: evidence for dip linkage during fault growth. Journal of Structural Geology 18, 249–263.
Martel, S.J., Boger, W.A., 1998. Geometry and mechanics of secondary fracturing around small three-dimensional faults in granitic rock. Journal of Geophysical Research 103, 21299–21308.
Martel, S.J., Pollard, D.D., Segall, P., 1988. Development of simple strike-slip fault zones, Mount Abbot quadrangle, Sierra Nevada, California. Geological Society of America Bulletin 100, 1451–1465.
Martel, S.J., 1997. Effects of cohesive zones on small faults and implications for secondary fracturing and fault trace geometry. Journal of Structural Geology 19, 835–847.
Mayeda, K., Walter, W.R., 1996. Moment, energy, stress drop, and source spectra of western United States earthquakes from regional coda envelopes. Journal of Geophysical Research 101, 11195–11208.
McGarr, A., 1988. On the state of lithospheric stress in the absence of applied tectonic forces. Journal of Geophysical Research 93, 13609–13617.
McKnight, E.T., 1940. Geology of area between Green and Colorado Rivers, Grand and San Juan Counties, Utah. United States Geological Survey Bulletin 908.
Nemat-Nasser, S., Oranratnachai, A., Keer, L.M., 1979. Spacing of water-free crevasses. Journal of Geophysical Research 84, 4611–4620.
Nicol, A.J., Watterson, J., Walsh, J.J., Childs, C., 1996. The shapes, major axis orientations and displacement patterns of fault surfaces. Journal of Structural Geology 18, 235–248.
Ohlmacher, G.C., Aydin, A., 1997. Mechanics of vein, fault and solution surface formation in the Appalachian Valley and Ridge, northeastern Tennessee, U.S.A.: implications for fault friction, state of stress and fluid pressure. Journal of Structural Geology 19927–19944.
Olig, S.S., Fenton, C.H., McCleary, J., Wong, I.G., 1996. The earthquake potential of the Moab Fault and its relation to salt tectonics in the Paradox Basin, Utah. In: Huffman Jr, A.C., Lund, W.R., Godwin, L.H. (Eds.), Geology and Resources of the Paradox Basin. Utah Geological Association Guidebook 25, pp. 251–264.
Ottesen Ellevset, S., Knipe, R.J., Olsen, T.S., Fisher, Q.J., Jones, G., 1998. Fault controlled communication in the Sleipner Vest Field, Norwegian continental shelf; detailed, quantitative input for reservoir simulation and well planning. In: Jones, G., Fisher,

Q.J., Knipe, R.J. (Eds.), Faulting, Fault Sealing and Fluid Flow in Hydrocarbon Reservoirs. Geological Society Special Publications 147, pp. 283–297.

Pollard, D.D., Segall, P., 1987. Theoretical displacements and stresses near fractures in rock: with applications to faults, joints, veins, dikes, and solution surfaces. In: Atkinson, B.K. (Ed.), Fracture Mechanics of Rock. Academic Press, London, pp. 277–349.

Price, N.J., Cosgrove, J.W., 1990. Analysis of Geological Structures. Cambridge University Press, Cambridge.

Price, N.J., 1966. Fault and Joint Development in Brittle and Semi Brittle Rock. Pergamon Press, Oxford.

Rawnsley, K.D., Rives, T., Petit, J.-P., Hencher, S.R., Lumsden, A.C., 1992. Joint development in perturbed stress fields near faults. Journal of Structural Geology 14, 939–951.

Reches, Z., Lockner, D.A., 1994. Nucleation and growth of faults in brittle rocks. Journal of Geophysical Research 99, 18159–18173.

Rippon, J.H., 1985. Contoured patterns of throw and hade of normal faults in the coal measures (Westphalian) of northeast Derbyshire. Proceedings of the Yorkshire Geological Society 45, 147–161.

Rispoli, R., 1981. Stress fields about strike-slip faults inferred from stylolites and tension gashes. Tectonophysics 75, T29–T36.

Rives, T., Rawnsley, K.D., Petit, J.-P., 1994. Analogue simulation of natural orthogonal joint set formation in brittle varnish. Journal of Structural Geology 16, 419–429.

Roering, J.J., Cooke, M.L., Pollard, D.D., 1997. Why blind thrust faults do not propagate to the Earth's surface: Numerical modeling of coseismic deformation associated with thrust-related anticlines. Journal of Geophysical Research 102, 11901–11912.

Rogers, R.D., Bird, D.K., 1987. Fracture propagation associated with dike emplacement at the Skaergaard intrusion, East Greenland. Journal of Structural Geology 9, 71–86.

Scholz, C.H., 1990. The Mechanics of Earthquakes and Faulting. Cambridge University Press, New York.

Segall, P., Pollard, D., 1980. Mechanics of discontinuous faults. Journal of Geophysical Research 85, 4337–4350.

Segall, P., Pollard, D.D., 1983. Nucleation and growth of strike-slip faults in granite. Journal of Geophysical Research 88, 555–568.

Shoemaker, E.M., Case, J.E., Elston, D.P., 1958. Salt anticlines of the Paradox Basin. In: Sanborn, A.F. (Ed.), Guidebook to the Geology of the Paradox Basin. Intermountain Association of Petroleum Geologists, Ninth Annual Field Conference, pp. 39–59.

Thomas, A.L., 1993. Poly3D: A three-dimensional, polygonal element, displacement discontinuity boundary element computer program with applications to fractures, faults, and cavities in the Earth's crust. MS thesis, Stanford University.

Trudgill, B., Cartwright, J., 1994. Relay-ramp forms and normal-fault linkages, Canyonlands National Park, Utah. Geological Society of America Bulletin 106, 1143–1157.

Vermilye, J.M., Scholz, C.H., 1998. The process zone: A microstructural view of fault growth. Journal of Geophysical Research 103, 12223–12237.

Willemse, E.J.M., Pollard, D.D., Aydin, A., 1996. Three-dimensional analyses of slip distributions on normal fault arrays with consequences for fault scaling. Journal of Structural Geology 18, 295–309.

Willemse, E.J.M., Peacock, D.C.P., Aydin, A., 1997. Nucleation and growth of strike-slip faults in limestones from Somerset, U.K. Journal of Structural Geology 19, 1461–1477.

Willis, G.C., 1986. Provisional geologic map of the Sego Canyon quadrangle, Grand County, Utah. Utah Geological and Mineral Survey Map 89, scale 1:24,000.

Zhao, G., Johnson, A.M., 1992. Sequence of deformations recorded in joints and faults, Arches National Park, Utah. Journal of Structural Geology 14, 225–236.